Article

Cell Chemical Biology

Profiling of drug resistance in Src kinase at scale uncovers a regulatory network coupling autoinhibition and catalytic domain dynamics

Graphical abstract

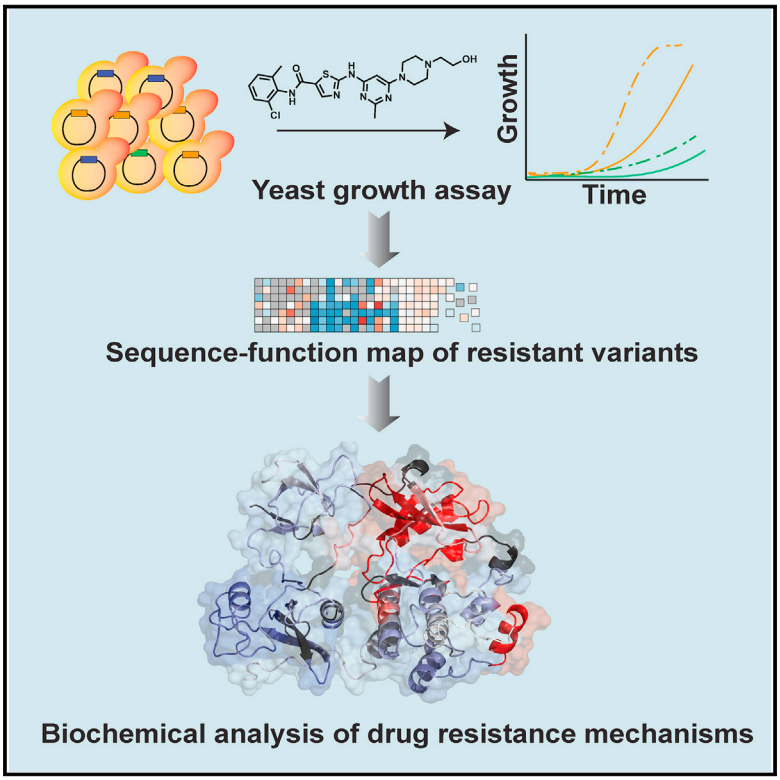

Highlights

- Mutational profiling in yeast allows characterization of drug resistance in Src
- Inhibitor resistance mutations are distributed throughout Src's catalytic domain
- Mutations that disrupt the regulation of Src often also lead to drug resistance
- Residues that modulate the dynamics and drug sensitivity of Src are revealed

Authors

Sujata Chakraborty, Ethan Ahler, Jessica J. Simon, ..., Miklos Guttman, Douglas M. Fowler, Dustin J. Maly

Correspondence

dfowler@uw.edu (D.M.F.), djmaly@uw.edu (D.J.M.)

In brief

Chakraborty et al. used a yeast-based screening method to quantify the resistance levels of 1000s of Src kinase mutants to diverse ATP-competitive inhibitors. Mutational profiling revealed that kinase inhibitor resistance can be obtained through multiple mechanisms, including by increasing the conformational dynamics of the kinase domain.

Chakraborty et al., 2023, Cell Chemical Biology *30*, 1–14
November 16, 2023
https://doi.org/10.1016/j.chembiol.2023.08.005

CellPress

Cell Chemical Biology

CellPress

Article

Profiling of drug resistance in Src kinase at scale uncovers a regulatory network coupling autoinhibition and catalytic domain dynamics

Sujata Chakraborty,[1,7] Ethan Ahler,[2,3,7] Jessica J. Simon,[1] Linglan Fang,[1] Zachary E. Potter,[1] Katherine A. Sitko,[2] Jason J. Stephany,[2] Miklos Guttman,[4] Douglas M. Fowler,[2,5,*] and Dustin J. Maly[1,6,8,*]

[1]Department of Chemistry, University of Washington, Seattle, WA 98195, USA
[2]Department of Genome Sciences, University of Washington, Seattle, WA 98195, USA
[3]Molecular and Cellular Biology, University of Washington, Seattle, WA 98195, USA
[4]Department of Medicinal Chemistry, University of Washington, Seattle, WA 98195, USA
[5]Department of Bioengineering, University of Washington, Seattle, WA 98195, USA
[6]Department of Biochemistry, University of Washington, Seattle, WA 98195, USA
[7]These authors contributed equally
[8]Lead contact
*Correspondence: dfowler@uw.edu (D.M.F.), djmaly@uw.edu (D.J.M.)
https://doi.org/10.1016/j.chembiol.2023.08.005

SUMMARY

Kinase inhibitors are effective cancer therapies, but resistance often limits clinical efficacy. Despite the cataloging of numerous resistance mutations, our understanding of kinase inhibitor resistance is still incomplete. Here, we comprehensively profiled the resistance of ~3,500 Src tyrosine kinase mutants to four different ATP-competitive inhibitors. We found that ATP-competitive inhibitor resistance mutations are distributed throughout Src's catalytic domain. In addition to inhibitor contact residues, residues that participate in regulating Src's phosphotransferase activity were prone to the development of resistance. Unexpectedly, we found that a resistance-prone cluster of residues located on the top face of the N-terminal lobe of Src's catalytic domain contributes to autoinhibition by reducing catalytic domain dynamics, and mutations in this cluster led to resistance by lowering inhibitor affinity and promoting kinase hyperactivation. Together, our studies demonstrate how drug resistance profiling can be used to define potential resistance pathways and uncover new mechanisms of kinase regulation.

INTRODUCTION

Small molecule, ATP-competitive kinase inhibitors have revolutionized the treatment of specific cancers.[1–3] Unfortunately, the efficacy of ATP-competitive kinase inhibitors is frequently limited by the development of resistance. Mechanisms of ATP-competitive kinase inhibitor resistance are often complex and heterogeneous[4,5] but point mutations that render a target kinase less sensitive to inhibition are common.[6] How do these kinase mutations result in resistance to an ATP-competitive inhibitor? One frequently observed mechanism is through the disruption of favorable binding interactions with the inhibitor. For example, mutation of the "gatekeeper" residue, which sits near the back of the ATP-binding pocket, to a bulkier residue that restricts the size of an adjacent hydrophobic pocket is one of the major pathways of resistance observed in the clinic for several kinases.[7,8] Similarly, other inhibitor contact residues are also commonly observed sites of ATP-competitive inhibitor resistance.[9] However, the mechanistic basis for many clinically observed mutations that do not directly influence drug binding is less clear, and even mutations that affect inhibitor binding can confer resistance through additional mechanisms. For example, while gatekeeper mutations often lead to a reduction in inhibitor affinity they can also decrease inhibitor efficacy by increasing the ability of ATP to compete for ATP-binding site occupancy[10] and have been shown to lead to hyperactivation of some tyrosine kinases.[11] Therefore, studies that allow the comprehensive profiling of inhibitor resistance are valuable in identifying potential sites of resistance and also providing new insight into kinase regulation and activity.

To obtain insight into different mechanisms of drug resistance, we used a deep mutational scanning (DMS) approach[12,13] to investigate the impact of nearly every mutation in Src kinase's catalytic domain on the efficacy of a panel of ATP-competitive inhibitors. Using this approach, we first established Src's pattern of resistance to the clinically approved inhibitor dasatinib. As expected, mutations at sites within the catalytic domain that interact with dasatinib were capable of conferring resistance. We also observed that residues involved in the autoinhibition of Src's phosphotransferase activity were particularly prone to

Please cite this article in press as: Chakraborty et al., Profiling of drug resistance in Src kinase at scale uncovers a regulatory network coupling auto-inhibition and catalytic domain dynamics, Cell Chemical Biology (2023), https://doi.org/10.1016/j.chembiol.2023.08.005

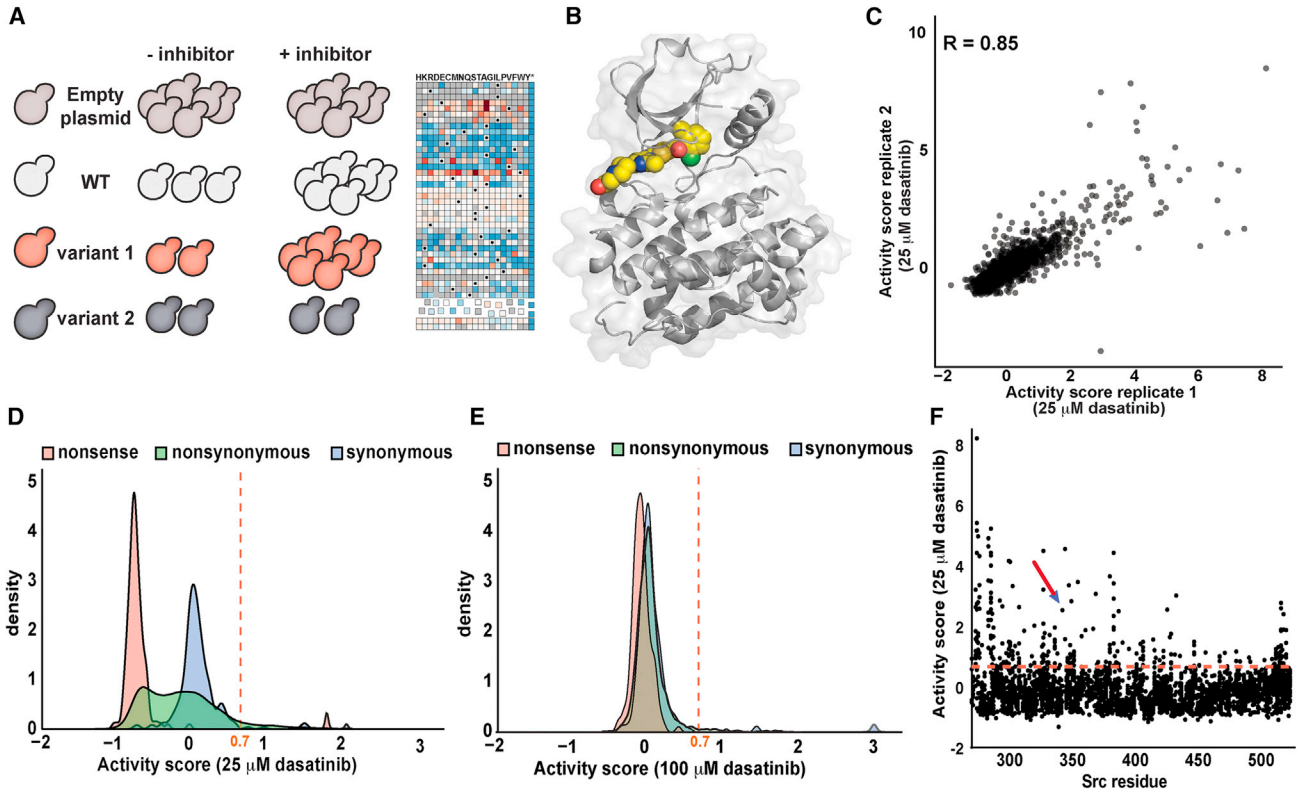

Figure 1. A yeast-based assay for the parallel analysis of drug resistance

(A) The yeast-based assay used to quantify the drug resistance of thousands of Src mutants.

(B) Co-crystal structure of dasatinib-bound Src (PDB: 3G5D) (*colored spheres*).

(C) Scatterplot showing the correlation between the activity scores obtained in 25 μM dasatinib-treated yeast for two independent transformations of the Src^{myr} variant library.

(D and E) Activity score distributions of all synonymous and nonsynonymous (missense and nonsense) Src^{myr} variants in yeast treated with 25 μM (D) or 100 μM (E) dasatinib. The red dashed line indicates the activity score value (>2 standard deviations above the mean of the synonymous WT distribution) we defined as dasatinib resistant.

(F) Scatterplot showing activity scores for every single amino acid substitution at every residue in Src's catalytic domain for yeast transformed with the Src^{myr} library and treated with 25 μM dasatinib (each black dot represents the activity score derived from averaging two replicates). The red dashed line indicates the dasatinib resistance cutoff. The T341I gatekeeper mutant is indicted by a red arrow. See also Tables S1 and S2; Figure S1.

the development of resistance to dasatinib. Next, we profiled a matched set of conformation-selective, ATP-competitive inhibitors to compare how resistance emerges in response to different modes of ATP-competitive inhibition. We identified a number of unique resistance mutations for each conformation-selective inhibitor and a shared set of residues that were highly susceptible to the development of resistance. Further investigation of a spatially defined cluster of residues located on the solvent-exposed N-terminal lobe of Src's catalytic domain, which we refer to as the β1/β2 resistance cluster, demonstrated that mutations at these residues were capable of reducing ATP-competitive inhibitor affinity. Biochemical analyses revealed that many mutations in the β1/β2 resistance cluster led to hyperactivation of Src's phosphotransferase activity and that this structural element also contributes to the autoinhibited state of Src by reducing the dynamics of the catalytic domain's N-terminal lobe, which resistance mutations release. Together, our results show how a previously unrecognized component of Src's auto-inhibitory regulatory network is a major site for the potential development of drug resistance.

RESULTS

A yeast-based growth assay for profiling drug resistance

To comprehensively profile the mechanisms of inhibitor resistance in Src, we used an assay that relies on the correlation between Src's phosphotransferase activity and its toxicity in *S. cerevisiae*.[14–16] We reasoned that it would be possible to determine the drug sensitivity of individual Src variants by measuring Src-mediated toxicity in the presence of various inhibitors (Figure 1A). Prior to performing a parallel analysis of Src mutants, we validated that diverse ATP-competitive inhibitors were capable of rescuing the growth inhibition that resulted from expressing wild-type (WT), myristoylated, full-length Src (Src^{myr}, see Table S1 for all Src constructs) in yeast (Figures S1A–S1D), and that growth rates correlated to inhibition of Src^{myr} (Figure S1E). Next, we utilized a previously published library[14] of single amino acid mutants of Src^{myr}'s catalytic domain (residues 270–519) that was generated using an inverse PCR saturation mutagenesis strategy.[17] To ensure that only single amino acid mutants were included in our analysis, we linked

Please cite this article in press as: Chakraborty et al., Profiling of drug resistance in Src kinase at scale uncovers a regulatory network coupling autoinhibition and catalytic domain dynamics, Cell Chemical Biology (2023), https://doi.org/10.1016/j.chembiol.2023.08.005

CellPress

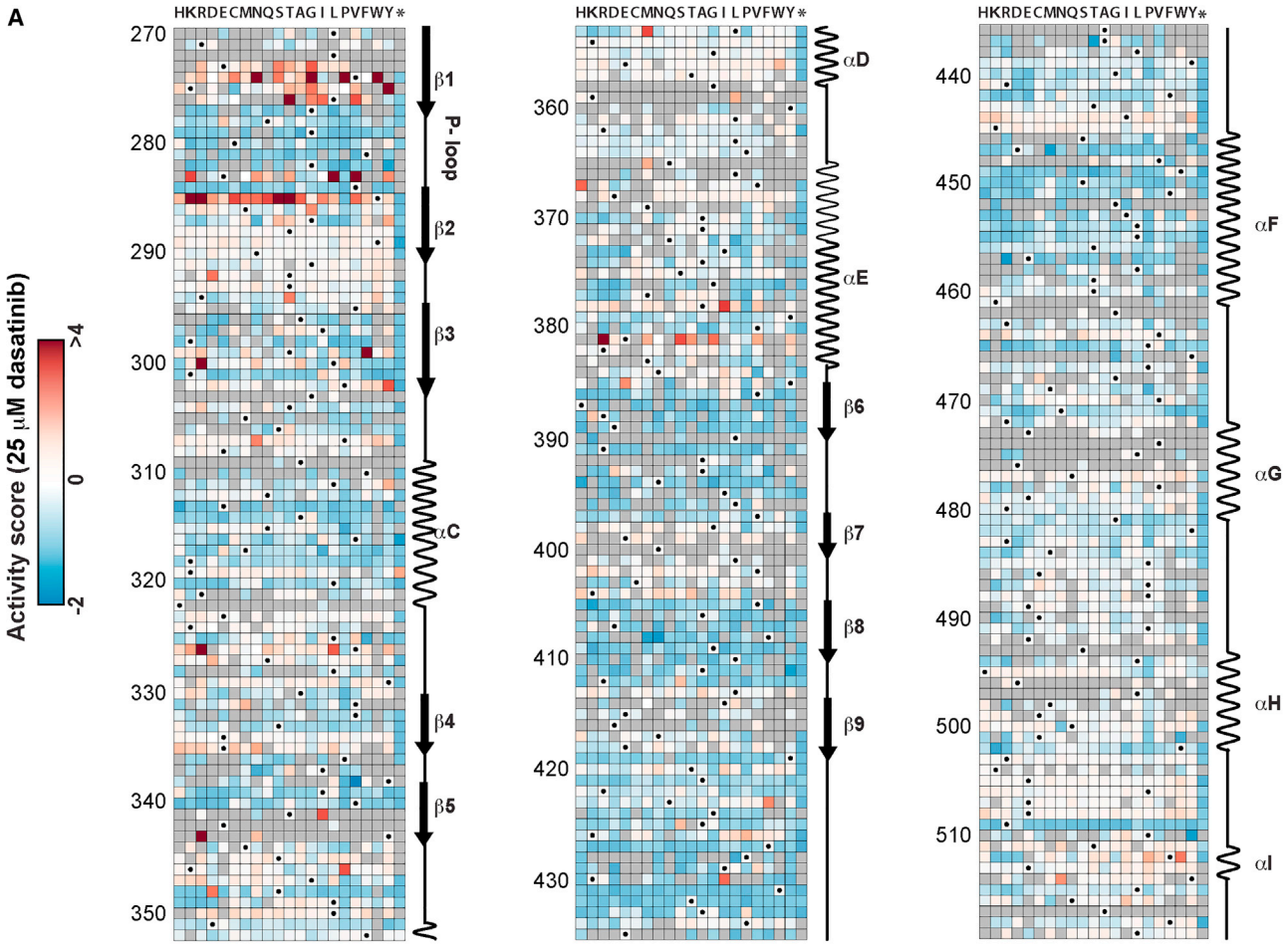

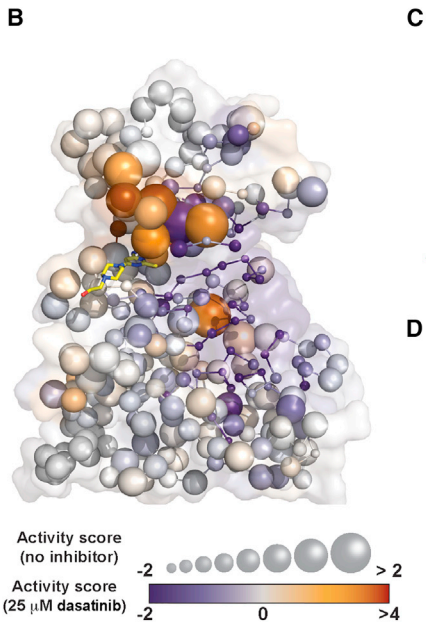

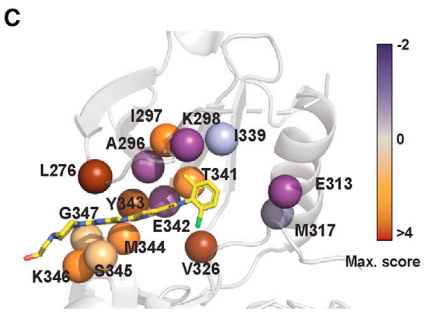

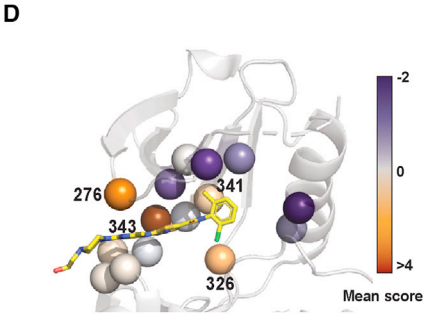

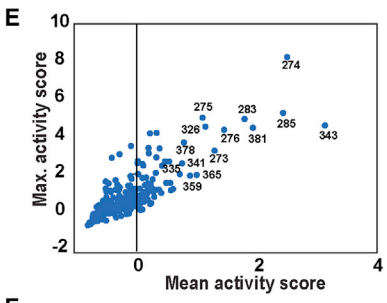

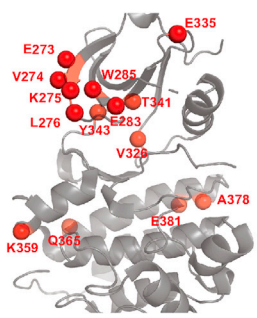

(legend on next page)

Please cite this article in press as: Chakraborty et al., Profiling of drug resistance in Src kinase at scale uncovers a regulatory network coupling autoinhibition and catalytic domain dynamics, Cell Chemical Biology (2023), https://doi.org/10.1016/j.chembiol.2023.08.005

each Src^{myr} variant to unique DNA barcodes using a subassembly strategy (Table S2).[18–20] In this Src^{myr} library (Table S3), each single amino acid mutant is represented by ~5 barcodes.

To profile dasatinib resistance (Figure 1B), we transformed the barcoded Src^{myr} library into yeast, collected yeast prior to inducing Src expression, and then performed outgrowth after induction of Src^{myr} expression in the presence of 25 or 100 μM dasatinib. For each dasatinib concentration, samples were collected at three early timepoints. At each timepoint and for yeast that were collected prior to Src induction, we extracted plasmid DNA, amplified barcodes, and then deeply sequenced the barcode amplicons to quantify the frequency of each Src variant. By regressing variant frequency data over time, we calculated activity scores for ~3,500 single amino acid Src mutants using the weighted least squares scoring method from the Enrich2 software package[21] at two different dasatinib concentrations by averaging two biological replicates (Figures 1C–1F, S1F, and S1G). For each concentration of dasatinib, we observed a good correlation between biological replicates, indicating that there was minimal uncoupling between Src variants and their associated barcodes during outgrowth with dasatinib. We defined a Src mutant as being drug resistant if it showed an activity score greater than two times the standard deviation from the mean of the synonymous distribution (Figures 1D and 1E). We found that patterns of dasatinib resistance looked similar for both dasatinib concentrations but with a lower correlation between biological replicates and a narrower distribution of activity scores for 100 μM dasatinib treatment (Figures 1D and 1E). Therefore, we further analyzed the data obtained from 25 μM dasatinib treatment, where a wider spectrum of mutational effects on resistance was apparent.

Profiling of dasatinib resistance in Src

We assembled our large-scale mutagenesis data into a sequence-activity map covering ~75% of all possible single mutants of Src's catalytic domain (Figure 2A; Table S3). About 8% of these single mutants were defined as dasatinib-resistant based on our classification criteria. Consistent with the notion that preservation of phosphotransferase activity is required for a mutation to confer drug resistance, we observed that almost all dasatinib-resistant mutations were either classified as activating (~65%) or WT-like (~30%) in a comprehensive analysis of Src's phosphotransferase activity that we previously performed (Figures 2B and S2A).[14] While elevated phosphotransferase activity appears to be a common dasatinib resistance mechanism, activity scores obtained in the absence or presence of dasatinib were not strictly correlated (Figures 2B and S2B), suggesting that diverse mechanisms of resistance were captured. Our sequence-activity map revealed that dasatinib-resistant mutations were distributed throughout the catalytic domain, especially in multiple residues in the β1 and β2 strands of the N-terminal lobe and the αD and αE helices of the C-lobe (Figures 2A and 2B). At many positions, only a few mutations conferred dasatinib resistance, while at a subset of residues most substitutions demonstrated dasatinib resistance (Figure 2A).

Mutations that perturb inhibitor contact residues in the ATP-binding pocket are a common mechanism of resistance to kinase inhibitors.[22] We explored whether our mutagenesis data captured this mechanism of dasatinib resistance by mapping the maximum and mean (position-averaged) activity scores that were obtained in the presence of 25 μM dasatinib onto the fifteen residues in Src's ATP-binding site that interact with dasatinib (Figures 2C and 2D). As expected, mutations at a number of residues that line the ATP-binding pocket led to substantial dasatinib resistance, including the well-characterized T341I gatekeeper mutation.[6,11] In addition, residues Leu276 (β1 strand), Val326 (located between the αC helix and β4 strand), and Tyr343 (hinge region) all showed high mean activity scores in the presence of 25 μM dasatinib (Figures 2D and 2E) and appeared to be highly susceptible to the development of resistance. In total, at least one substitution led to resistance at two-thirds of the residues that interact with dasatinib, consistent with the ATP-binding pocket being a site of significant potential drug resistance. Our results are consistent with a recent screen of cyclin-dependent kinase 6 (CDK6)'s resistance to the ATP-competitive inhibitor palbociclib.[22] Despite the different binding poses of palbociclib and dasatinib within the ATP-binding pockets of CDK6 and Src, respectively, resistance mutations occurred at many of the same contact residues, and a similar percentage of contact residues were capable of acquiring inhibitor resistance (Figures S2C and S2D). Although there are no inhibitors in the clinic that elicit their mechanism of action through the inhibition of Src, we compared our results to a recent study that characterized 94 patient-derived and resistance-associated mutants of the tyrosine kinase Abl, which possesses a kinase domain that is highly similar to that of Src.[23] We observed at least one resistance mutation at six (Leu276, V295, V316, T341, Y343, and A378) of the nine positions in Abl's kinase domain that

Figure 2. Mapping of dasatinib resistance mutations in Src

(A) Sequence-activity score map for all residues in Src's catalytic domain for the Src^{myr} variant library treated with 25 μM dasatinib. Each row represents a residue in Src's catalytic domain (starting at residue 270 and ending at residue 519) and each column represents an amino acid substitution (* = nonsense mutation). Black dots represent the wild-type amino acid and gray tiles indicate missing data. Secondary structure and functional motif annotations were obtained from the ProKinO database.

(B) Mean (position-averaged) activity scores for each residue in Src's catalytic domain (PDB: 3G5D) for the Src^{myr} variant library in the absence or presence of dasatinib. Sphere size indicates position-averaged activity scores in the absence of dasatinib[14]; color indicates position-averaged activity scores in the presence of 25 μM dasatinib (*this study*). Nonsense mutants were excluded from the average score.

(C) Co-crystal structure of dasatinib-bound Src (PDB: 3G5D), showing the maximum activity scores for all dasatinib-interacting residues in the presence of 25 μM dasatinib.

(D) Co-crystal structure of dasatinib-bound Src (PDB: 3G5D), showing the mean activity scores for all dasatinib-interacting residues in the presence of 25 μM dasatinib.

(E) Correlation plot of maximum activity scores and mean activity scores in the presence of 25 μM dasatinib for each residue in Src's catalytic domain.

(F) Crystal structure (PDB: 3G5D) of Src's catalytic domain with the fourteen residues that were defined as "resistance prone" shown as red spheres. See also Table S3 and Figure S2.

Please cite this article in press as: Chakraborty et al., Profiling of drug resistance in Src kinase at scale uncovers a regulatory network coupling autoinhibition and catalytic domain dynamics, Cell Chemical Biology (2023), https://doi.org/10.1016/j.chembiol.2023.08.005

contained mutations (14 in total) that were found to lead to a >2-fold decrease in dasatinib binding (Figure S2E). Consistent with the similarities between Src's and Abl's ATP-binding sites but divergence in certain aspects of their regulatory mechanisms, positions where dasatinib resistance was shared between Src and Abl are mainly clustered around the ATP-binding cleft.

Our sequence-activity map shows that there are several residues where numerous substitutions led to dasatinib resistance, suggesting that they represent sites that are particularly prone to the development of drug resistance. To quantitatively identify resistance-prone sites, we determined all residues in Src's catalytic domain that demonstrated mean (position-averaged) activity scores greater than our defined drug-resistance cutoff for an individual mutant in the presence of 25 μM dasatinib (Figures 2F and S2F). In total, fourteen residues meet the "resistance-prone" definition. While four of the fourteen resistance-prone residues (Leu276, Val326, Thr341, and Tyr343) interact with dasatinib (Figures 2C and 2D), the remaining ten either possess sidechains that are directed away from the ATP-binding site or are distal to the site of dasatinib binding. We previously observed that eight of the resistance-prone residues that do not interact with dasatinib contained a large number of activating mutations in the absence of dasatinib and are likely involved in the regulation of Src's phosphotransferase activity.[14] Ala378 and Glu381 are components of the regulatory αF pocket in the C-terminal lobe that contributes to the autoinhibition of Src's phosphotransferase activity through an interaction with the N-terminal SH4 domain. Residues Glu273, Val274, Lys275, Glu283, and Trp285 form a solvent-exposed, spatially defined cluster of residues located on the β1 and β2 strands of the N-terminal lobe and appear to contribute to Src's autoinhibition by an unknown mechanism. Thus, elevated phosphotransferase activity appears to be a general mechanism for acquiring dasatinib resistance in Src.

Src mutational resistance to different modes of ATP-competitive inhibition

We further explored the intersection between the regulation of Src's phosphotransferase activity and drug resistance by determining how resistance arises in response to different modes of ATP-competitive inhibition (Figure S3A).[24–27] We profiled our Src variant library in the presence of each of a matched set of pyrazolopyrimidine-based, ATP-competitive inhibitors that stabilize structurally distinct conformations of Src's ATP-binding site (Figure 3A). Inhibitor **1** contains a 3-phenol at the C-3 position of the pyrazolopyrimidine scaffold that can potentially form a hydrogen-bond with the sidechain of Glu313 in the αC helix, leading to stabilization of the active conformation (αC helix-in; Figure S3A). Inhibitor **2** contains a pharmacophore at the C-3 position that promotes the outward rotation of the αC helix to an inactive conformation (αC helix-out). We also attempted to profile an inhibitor (inhibitor **3**) that contains a pharmacophore at the C-3 position of the pyrazolopyrimidine scaffold that stabilizes a flipped, inactive conformation of Src's activation loop (DFG-out) but is otherwise identical to inhibitors **1** and **2**. However, inhibitor **3** did not achieve sufficiently high intracellular concentrations in yeast to inhibit WT Src^{myr}. Therefore, we used inhibitor **4**, an analog of **3** that achieved high enough concentrations in yeast to inhibit WT Src^{myr} (Figure S1D), for our profiling experiments.

After transforming the Src^{myr} variant library into yeast, we performed outgrowth in the presence of **1**, **2**, or **4** and collected samples at early timepoints. For each inhibitor, we calculated normalized activity scores for ~3,500 Src mutants (Figure S3B; Table S4). A Src variant was defined as being resistant if its activity score in the presence of a specific inhibitor was greater than three times the standard deviation from the mean of the synonymous distribution. Using this definition, we identified 107, 86, and 114 Src mutants that were resistant to **1**, **2**, and **4**, respectively (Figure S3B). Similar to Src's resistance to dasatinib, almost all variants that were resistant to **1**, **2**, or **4** were either classified as activating or WT-like in our previous analysis of Src's phosphotransferase activity (Figure S3C). In comparing the overlap between resistance mutations, we observed 22 mutations occurring at eight residues that were resistant to all three conformation-selective inhibitors (Figures 3B and S3D). Inhibitors **1** and **4** shared the highest overlap (~75%) in resistance mutations, suggesting that their shared ability to stabilize an active conformation of Src's αC helix makes them susceptible to similar mechanisms of resistance. Despite these similarities, we observed that ~25–45% of all resistance mutations for a particular inhibitor were unique (Figure 3C), revealing resistance mechanisms that are likely specific to different modes of conformation-selective inhibition.

To provide a comprehensive overview of which regions are generally resistant to different modes of ATP-competitive inhibition, we mapped mean activity scores for each inhibitor onto the catalytic domain of Src (Figure 3E). Inhibitors **1** and **4** shared similar patterns of resistance, with the solvent-facing N-terminal lobe of the catalytic domain representing the main region of resistance. While residues in the same region of Src's N-terminal lobe also demonstrated resistance to **2**, unique resistance mutations to this αC helix-out-stabilizing inhibitor were also observed through the entirety of Src's kinase domain. In particular, three residues (Leu300, Ile337, and Leu413) contained multiple mutations that uniquely conferred strong resistance to **2**. Leu300 is located on the linker that connects the αC helix to the β-sheet of the N-terminal lobe and Ile337 is located on the face of the β4 strand that is directed toward helix αC. A plausible explanation for how mutations at these residues confer resistance is that they negatively influence the ability of helix αC to adopt the inactive "out" conformation that is required for inhibitor **2** to be accommodated in Src's ATP-binding pocket.[28]

We observed six residues (Leu276, Trp285, Val326, Thr341, Tyr343, and Glu381) that fulfill our definition of being resistance-prone to all three conformation-selective inhibitors (Figure 3E and S3D). These six residues were also classified as being resistance-prone for dasatinib (Figure 2F). The sidechains of Leu276, Val326, Thr341, and Tyr343 are all directed toward Src's ATP-binding pocket and mutations at these residues most likely confer resistance by perturbing inhibitor contacts. For example, mutations at the gatekeeper residue that restrict the size of the ATP-binding pocket or lead to the loss of hydrophobic interactions with inhibitors are commonly observed clinical resistance mutations.[23] We speculated that mutations at Val326, which contains a sidechain that is directed toward the adenine ring of ATP and makes hydrophobic contacts with dasatinib and other inhibitors (Figure S3E), provided resistance through a similar mechanism. To test this prediction, we performed phosphotransferase activity

Please cite this article in press as: Chakraborty et al., Profiling of drug resistance in Src kinase at scale uncovers a regulatory network coupling autoinhibition and catalytic domain dynamics, Cell Chemical Biology (2023), https://doi.org/10.1016/j.chembiol.2023.08.005

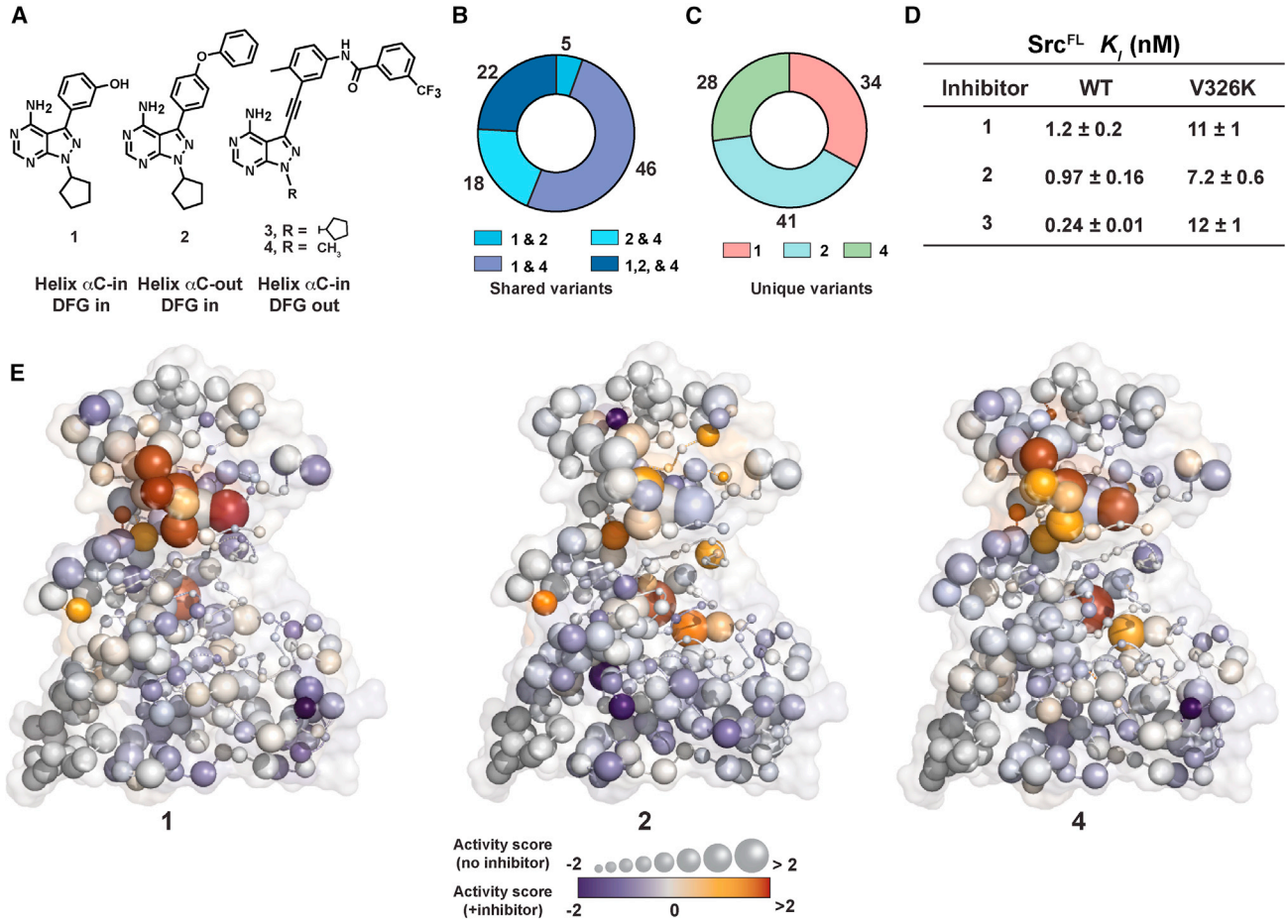

Figure 3. Resistance to conformation-selective, ATP-competitive inhibitors

(A) Structures of the conformation-selective, ATP-competitive inhibitors that were profiled.

(B) Donut plot showing the number of shared inhibitor-resistant mutants.

(C) Donut plot showing the number of unique inhibitor-resistant mutants for inhibitors **1**, **2**, and **4**.

(D) K_I values (n = 3, mean ± SEM) of inhibitors **1**–**3** for purified WT and V326K Src^{FL} constructs obtained using an *in vitro* activity assay.

(E) Mean activity scores for each residue in Src's catalytic domain (PDB: 3G5D) for the Src^{myr} variant library treated with **1** (*left*), **2** (*middle*), or **4** (*right*) and in absence of inhibitor (data from a previous study[14]). Mean activity scores in the presence of inhibitor are represented as color, while activity scores in the absence of inhibitors are represented by sphere size. See also Table S4 and Figure S3.

and inhibition assays with WT and an inhibitor-resistant variant (V326K) of purified full-length Src (Src^{FL}). We observed that purified V326K Src^{FL}'s K_M for ATP (K_M[ATP]) and phosphotransferase activity were very similar to WT Src^{FL}'s (Figure S3F and S3G). Consistent with the V326K mutation leading to reduced inhibitor affinity, purified V326K Src^{FL} displayed K_I values for inhibitors **1**, **2**, and **3** that were 5- to 50-fold higher than WT Src^{FL} (Figure 3D). Interestingly, the tyrosine kinases BCR-Abl, Alk, and c-KIT also contain a valine at an equivalent position in their ATP-binding sites and drug-resistant mutations have been observed at this position in the clinic (Figure S3H). Thus, this region of the ATP-binding site appears to be a site of inhibitor resistance for a number of tyrosine kinases.

Characterization of a resistance-prone cluster of residues in the N-terminal lobe of Src's catalytic domain

Six residues (Glu273, Val274, Lys275, Leu276, Glu283, and Trp285) that possess multiple drug-resistant mutants form a spatially defined cluster on the top face of the β1 and β2 stands in the N-terminal lobe of Src's catalytic domain (Figures 4A and S4A–S4E). Despite the high number of mutations that conferred resistance at the six residues within this cluster, which we hereafter refer to as the β1/β2 resistance cluster, the sidechains of all but Leu276 are solvent exposed and directed away from the ATP-binding site of Src (Figure S4A). Therefore, we were curious why this cluster of solvent-exposed residues is so prone to the development of drug resistance. To determine whether mutations within the β1/β2 resistance cluster confer resistance by reducing Src's affinity for ATP-competitive inhibitors, we determined the K_I values of **1**–**3** for purified Src^{FL} constructs containing drug-resistant E283M or W285T mutations (Figure 4B). We found that the presence of either the E283M or W285T mutation led to increased K_I values for **1**–**3** relative to WT Src^{FL} but had a negligible effect on the K_M for ATP (Figures 4B and S4G). Furthermore, we found that both mutations conferred similar levels of inhibitor resistance. Therefore, mutations in the β1/β2

Please cite this article in press as: Chakraborty et al., Profiling of drug resistance in Src kinase at scale uncovers a regulatory network coupling autoinhibition and catalytic domain dynamics, Cell Chemical Biology (2023), https://doi.org/10.1016/j.chembiol.2023.08.005

CellPress

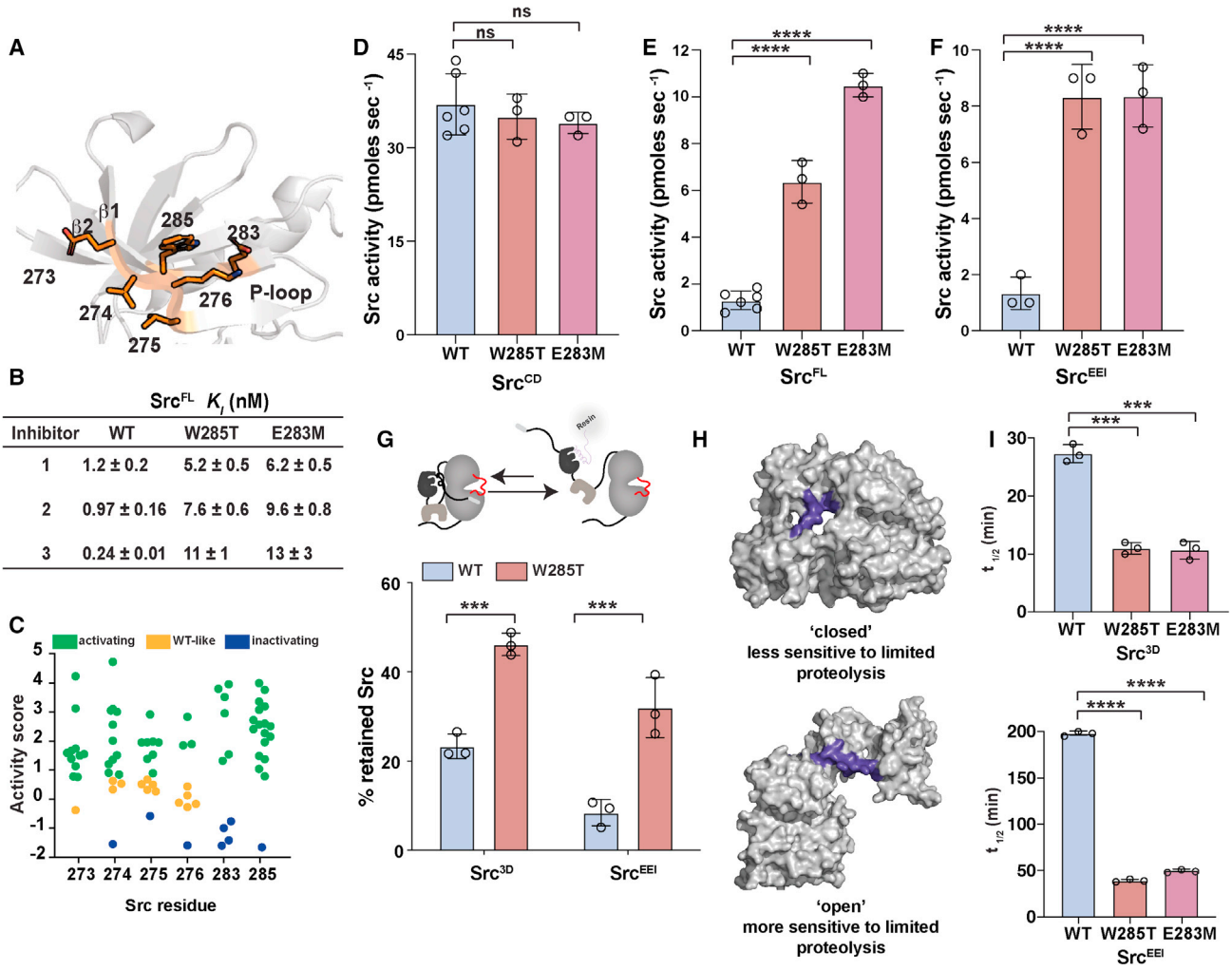

Figure 4. Biochemical characterization of the β1/β2 resistance cluster

(A) Top-down view of the N-terminal lobe of Src's catalytic domain (PDB: 1Y57) with the sidechains of residues in the β1/β2 resistance cluster shown (*orange*).

(B) K_I values of **1**–**3** for purified WT, E283M, and W285T Src^{FL} (n = 3, mean ± SEM) using an *in vitro* assay.

(C) Activity scores for every substitution at each residue in the β1/β2 resistance cluster in the absence of an inhibitor determined in a previous study.[14]

(D) Phosphotransferase activity of purified WT, W285T, or E283M Src^{CD} (n = 3–5, mean ± SEM, ns = non-significant, $p > 0.05$).

(E) Phosphotransferase activity of purified WT, W285T, or E283M Src^{FL} determined with an *in vitro* assay (n = 3–5, mean ± SEM, ****$p < 0.0001$).

(F) Phosphotransferase activity of purified WT, W285T, or E283M Src^{EEI} determined with an *in vitro* assay (n = 3, mean ± SEM, ****$p < 0.0001$).

(G) Schematic of the *in vitro* SH3 domain pulldown assay. Percent retained purified WT or W285T Src^{3D} (left, n = 3, mean ± SEM, ***$p < 0.001$) and WT or W285T Src^{EEI} (right, n = 3, mean ± SEM, ****$p < 0.0001$) in the SH3 domain pull-down assay.

(H) Crystal structure (PDB: 2SRC) of Src^{3D} in the closed (*top*) and open (bottom) global conformations. The SH2-catalytic domain linker (*violet*) of the open conformation of Src^{3D} is more sensitive to proteolysis than the closed global conformation.

(I) Half-life values of purified WT, E283M, or W285T Src^{3D} (*top*, n = 3, mean ± SEM, ***$p < 0.001$) and WT, E283M, or W285T Src^{EEI} (*bottom,* n = 3, mean ± SEM, ****$p < 0.0001$) in the limited proteolysis assay. See also Figure S4.

resistance cluster confer resistance, in part, by lowering the affinity of inhibitors for Src's ATP-binding site.

Residues in the β1/β2 resistance cluster modulate autoinhibition of Src

We previously observed that all six residues within the β1/β2 resistance cluster also contained multiple activating mutations in the absence of inhibitors (Figure 4C),[14] suggesting that this region may serve a role in modulating Src's phosphotransferase activity. Therefore, we next determined how activating mutations in the β1/β2 resistance cluster influence Src's phosphotransferase activity with purified Src constructs (Figure S4F). Interestingly, we found that the E283M and W285T mutations had a negligible effect on the phosphotransferase activity of a construct (Src^{CD}) consisting solely of the catalytic domain of Src (Figures 4D and S4G). However, we observed that both mutations were activating in the context of Src^{FL} (Figure 4E), suggesting that activating mutations in the β1/β2 resistance cluster release regulatory domain-mediated autoinhibition. Consistent with the β1/β2 resistance cluster influencing regulation mediated

Please cite this article in press as: Chakraborty et al., Profiling of drug resistance in Src kinase at scale uncovers a regulatory network coupling auto-inhibition and catalytic domain dynamics, Cell Chemical Biology (2023), https://doi.org/10.1016/j.chembiol.2023.08.005

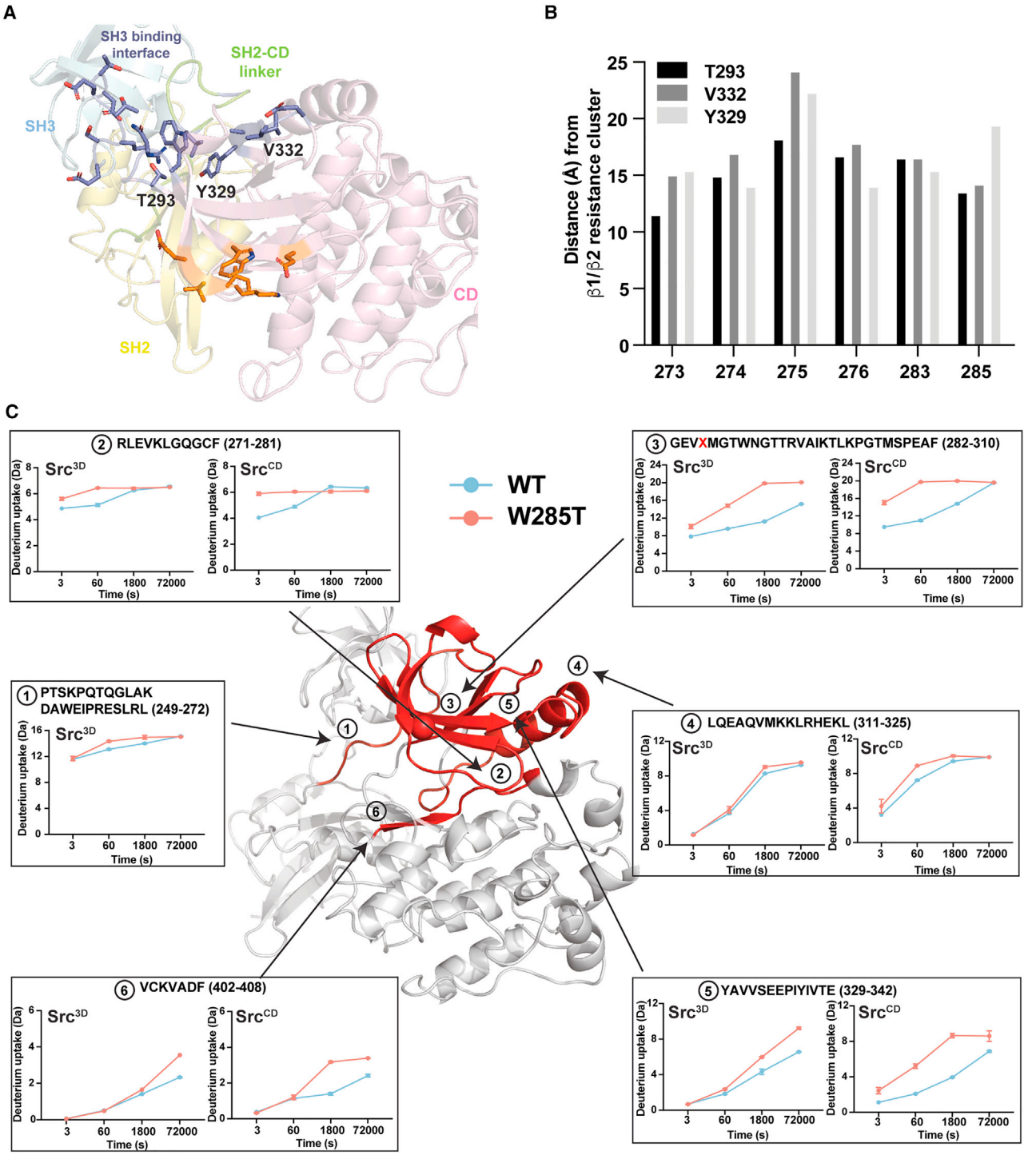

Figure 5. Conformational dynamics of W285T Src

(A) Structure of autoinhibited Src^{3D} (PDB: 2SRC) showing the sidechains of residues in the β1/β2 resistance cluster (*orange*) and the sidechains of residues in the nearest regulatory interface (*blue*, SH3) in Src's catalytic domain.

(B) Plot showing the distances between the β-carbons of the three residues in the SH3 domain regulatory interface closest to the β1/β2 resistant cluster and the β-carbons of residues in the β1/β2 resistant cluster.

(legend continued on next page)

Please cite this article in press as: Chakraborty et al., Profiling of drug resistance in Src kinase at scale uncovers a regulatory network coupling autoinhibition and catalytic domain dynamics, Cell Chemical Biology (2023), https://doi.org/10.1016/j.chembiol.2023.08.005

by Src's SH2 and SH3 domains, and not the N-terminal SH4 and unique domains, the E283M and W285T mutations showed a similar level of activation relative to WT in a Src^{3D} construct, Src^{EEI}, that possesses SH2 domain interaction-enhancing mutations in the C-terminal tail that promote a similar level of autoinhibition as Src^{FL} (Figure 4F). Together, our data support a model wherein residues in the β1/β2 resistance cluster reinforce the autoinhibition provided by the SH2 and SH3 domain regulatory apparatus, which activating mutations release.

We speculated that activating mutations in the β1/β2 resistance cluster increase Src's phosphotransferase activity by reducing levels of intramolecular SH2 and SH3 domain regulatory engagement. To test this prediction, we assessed how mutations affect intramolecular regulatory domain engagement levels with two biochemical assays. First, we measured intramolecular SH3 domain engagement levels with an immobilized SH3 domain ligand pull-down assay (Figure 4G). Consistent with activating β1/β2 resistance cluster mutations leading to increased phosphotransferase activity by reducing the autoinhibitory engagement of Src's regulatory apparatus, W285T Src^{3D}'s association with an immobilized SH3 domain ligand was more than 2-fold greater than WT Src^{3D}'s (Figures 4G and S4H). Furthermore, the W285T mutation dramatically increased the ability of the more regulatory domain-engaged Src^{EEI} construct to intermolecularly interact with the immobilized SH3 domain ligand relative to WT Src^{EEI} (Figures 4G and S4H). We next used the rate of proteolysis of the flexible linker that connects Src's SH2 domain to its CD (SH2-CD linker) by thermolysin to characterize how β1/β2 resistance cluster mutations affect intramolecular regulatory domain engagement. Previous studies have demonstrated an inverse correlation between the rate of thermolysin cleavage, measured as intact protein half-life ($t_{1/2}$), of the SH2-CD linker and intramolecular SH2 and SH3 regulatory domain engagement levels (Figure 4H).[25,29] Concordant with the SH3 domain pull-down results, the SH2-CD linkers of E283M and W285T Src^{3D} were proteolyzed 2–3 times more rapidly than WT Src^{3D} (Figure 4I and S4I). The E283M and W285T mutations also dramatically increased the rate of proteolytic cleavage of Src^{EEI}'s SH2-CD linker (Figures 4I and S4J). Thus, residues in the β1/β2 resistance cluster appear to influence the level of intramolecular engagement of Src's SH2 and SH3 domains.

The W285T mutation promotes a more dynamic N-terminal lobe of Src

While our biochemical analyses suggest that activating mutations in the β1/β2 resistance cluster increase Src's phosphotransferase activity by promoting a more open, regulatory domain-disengaged global conformation, the mechanistic basis for this effect was unclear. To the best of our knowledge, no previous structural or biochemical studies have suggested that residues within the β1/β2 resistance cluster participate in regulatory interactions. Furthermore, residues in the β1/β2 resistance cluster are separated by >10 Å from the nearest regulatory interface of autoinhibited Src (Figures 5A and 5B). Thus, we performed Hydrogen-Deuterium eXchange Mass Spectrometry (HDX-MS) on Src^{3D} to provide an unbiased analysis of how activating β1/β2 resistance cluster mutations affect the global conformational dynamics of Src.[26,30,31] Specifically, we compared the deuterium backbone exchange kinetics of W285T Src^{3D} relative to WT Src^{3D}. We subjected identical concentrations of WT Src^{3D} and W285T Src^{3D} to standard D_2O exchange conditions and samples were quenched and processed at various timepoints using established methods. Using this protocol, we were able to monitor the exchange kinetics of peptic peptides covering ~85% of WT Src^{3D}'s and W285T Src^{3D}'s sequence (Table S5).

Mapping differences in deuterium exchange kinetics between W285T Src^{3D} and WT Src^{3D} onto a structure of autoinhibited Src^{3D} (Figure 5C) revealed that a large portion of Src's catalytic domain in W285T Src^{3D} underwent faster exchange kinetics than in WT Src^{3D}. Consistent with β1/β2 resistance cluster mutations leading to a reduction in the intramolecular engagement of Src's regulatory SH2 and SH3 domain apparatus (Figures 4G and 4I), peptic peptides covering the SH2-catalytic domain linker (peptide 1: 249–272) and the SH3 domain interface (peptide 3: 282–310) of autoinhibited Src demonstrated increased solvent accessibility in W285T Src^{3D} relative to WT Src^{3D}. Furthermore, the W285T mutation also increased exchange kinetics in the activation loop (peptide 6: 402–408) and most of the N-terminal lobe of Src's catalytic domain. Thus, β1/β2 resistance cluster mutations appear to promote a more open, regulatory domain-disengaged global state of Src and a dramatically more dynamic N-terminal lobe in Src's catalytic domain.

The large number of peptic peptides that displayed faster exchange kinetics in W285T Src^{3D} relative to WT Src^{3D} made it difficult to discriminate which differences resulted from localized effects on dynamics versus those that arose from a more open and regulatory domain-disengaged conformational state of Src^{3D}. Therefore, we performed a comparative HDX-MS analysis with Src constructs (W285T Src^{CD} and WT Src^{CD}) that lack the SH2 and SH3 domain regulatory apparatus. We observed that the W285T mutation led to faster exchange kinetics for a comparable region of Src's catalytic domain in Src^{CD} to that of Src^{3D} (Figure 5C). As in Src^{3D}, the peptic peptide that contains the W285T mutation (peptide 3) demonstrated markedly increased exchange kinetics in W285T Src^{CD} relative to WT Src^{CD}. In addition to peptic peptide 3, we found that the peptic peptides comprising the remainder of the catalytic domain's N-terminal lobe (Figure 5C) also demonstrated greatly increased exchange kinetics in W285T Src^{CD}, suggesting that this mutation directly increases the dynamics of this entire region. Interestingly, a peptic peptide spanning Src's αC helix (peptide 4: 311–325) demonstrated a large difference in dynamics between W285T Src^{CD} and WT Src^{CD}. Given the requirement that Src's αC helix must adopt an ordered "out" conformation for the catalytic domain to form a high affinity interaction with the SH2-catalytic domain linker and the SH3 domain in the autoinhibited form of

(C) HDX-MS analysis of purified Src^{3D} (WT compared to W285T) and Src^{CD} (WT compared to W285T). Deuteration differences between WT and W285T Src^{3D} and Src^{CD} are plotted on the crystal structure of Src^{3D} (PDB: 2SRC). Regions that show increased deuterium uptake (significant differences in exchange were assessed using the hybrid significance threshold at 99% CI as well as consistency among all observed overlapping peptides)[38] in W285T Src^{3D} and/or Src^{CD} relative to WT Src^{3D} and/or Src^{CD}, respectively, are shown in red, while regions that show no difference are shown in white. Values shown at each timepoint represent the mean ± SEM (n = 3). See also Table S5.

Please cite this article in press as: Chakraborty et al., Profiling of drug resistance in Src kinase at scale uncovers a regulatory network coupling autoinhibition and catalytic domain dynamics, Cell Chemical Biology (2023), https://doi.org/10.1016/j.chembiol.2023.08.005

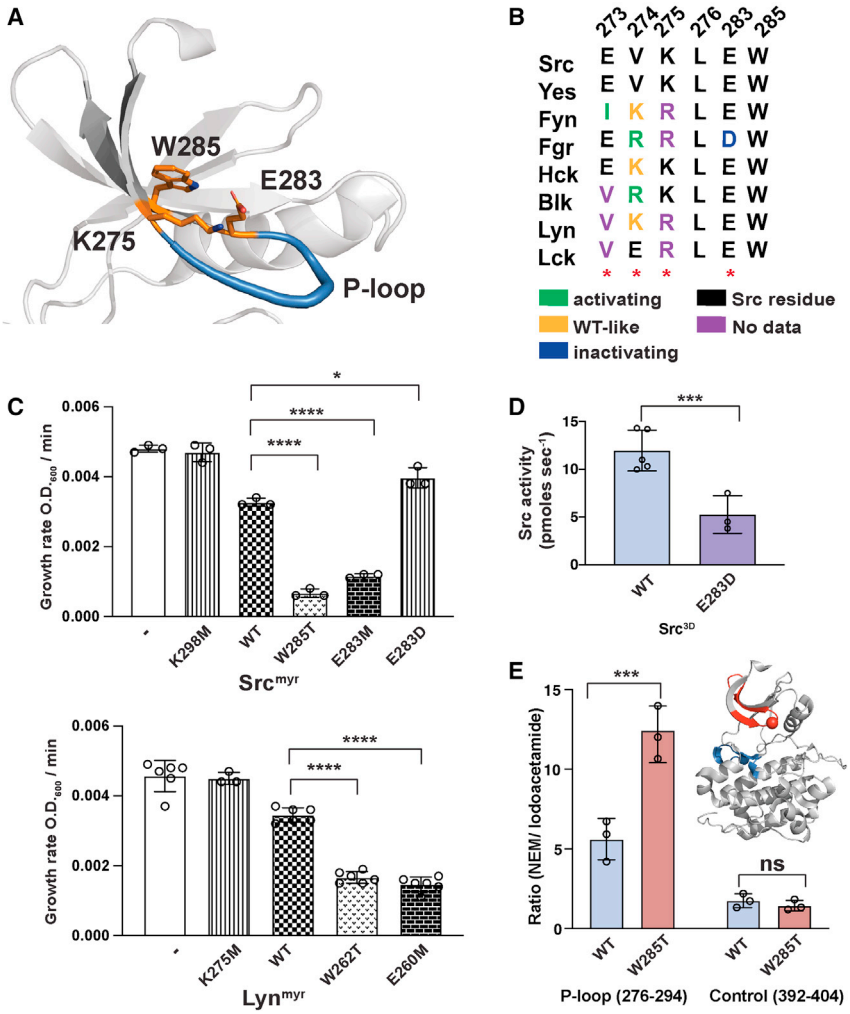

Figure 6. β1/β2 resistance cluster mutations influence the dynamics of Src's P-loop

(A) Structure of the N-terminal lobe of Src's catalytic domain (PDB: 1Y57) showing the flexible region of Src's P-loop (*blue*) and K275, E283, and Trp285 as orange sticks.

(B) Sequence alignment of SFK β1/β2 resistance cluster residues. Classifications (activating, WT-like, or inactivating) are from a previous study.[14]

(C) Growth rates of yeast expressing either (*top*) Src^{myr} (kinase dead (K298M), WT, W285T, E283M, or E283D, n = 3) or (*bottom*) Lyn^{myr} (kinase dead (K275M), WT, W262T, or E260M, n = 3–6, mean ± SEM, *p < 0.05, ****p < 0.0001).

(D) Phosphotransferase activity of purified WT and E283D Src^{3D} (n = 3–5, mean ± SEM, ***p < 0.001) determined with an *in vitro* assay.

(E) Peak intensity ratios of N-ethylmaleimide (NEM) to iodoacetamide labeling of a Cys-containing tryptic peptide in Src's P-loop (n = 3, mean ± SEM, ***p < 0.001) and a Cys-containing control tryptic peptide (n = 3, ns = non-significant, p > 0.05) from purified WT and W285T Src^{CD}. The inset shows Src's catalytic domain (PDB: 1Y57) with the Cys-containing P-loop (*red*) and the Cys-containing control peptide (*blue*). See also Figure S5.

Src, the ability of activating mutations in the β1/β2 resistance cluster to directly increase the dynamics of this region provides a plausible mechanism for the reduced intramolecular regulatory domain engagement we observed in our biochemical assays (Figure 4). Together, our results support a model where residues in the β1/β2 resistance cluster promote autoinhibitory interactions by restricting the conformational flexibility of the N-terminal lobe, including the αC helix. Activating mutations in the β1/β2 resistance cluster increase the dynamics of the N-terminal lobe, resulting in reduced autoinhibition and a subsequent increase in phosphotransferase activity.

Mutations in the β1/β2 resistance cluster affect the dynamics of Src's P-loop

Residues in the β1/β2 resistance cluster are part of a structured region that flanks Src's phosphate-binding loop (P-loop) (Figure 6A). A previous study showed that a salt bridge between β1/β2 resistance cluster residues K252 and E260 in the Src Family Kinase (SFK) Lyn (equivalent to K275 and E283 in Src, respectively) appears to affect the dynamics of its P-loop and that mutations that disrupt this electrostatic interaction modulate Lyn's phosphotransferase activity.[32] All SFKs contain amino acids that can potentially form a salt bridge at positions equivalent to K275 and E283 in Src (Figure 6B) and we observed that, like Src^{myr}, a salt bridge-disrupting mutation (E260M) increased the activity of Lyn^{myr} relative to its WT variant in yeast (Figures 6C and S5A). Consistent with the potential importance of the salt bridge between K275 and E283 in influencing Src's phosphotransferase activity, we found that Src constructs that contain a mutation (E283D) that preserves, or potentially enhances, an electrostatic interaction with K275 showed reduced catalytic activity in yeast (Figures 6C and S5A) and in *in vitro* activity assays with purified Src constructs (Figure 6D) relative to WT. The reduction in phosphotransferase activity of E283D Src^{3D} correlated with increased levels of regulatory domain engagement (Figure S5B). Together, previous data and our results suggest that a conserved salt bridge located within the β1/β2 resistance cluster affects the dynamics of SFK P-loops, which influences their phosphotransferase activities.

We speculated that activating mutations at other positions in the β1/β2 resistance cluster could also influence the dynamics of Src's P-loop like salt bridge-disrupting mutations. Indeed, our HDX-MS results demonstrated that the two peptic peptides that span the entirely of Src's P-loop showed greatly increased exchange dynamics in W285T Src^{3D} and Src^{CD} (Figure 5C). However, the large size of the peptic peptides obtained in our HDX-MS workflow made it difficult to determine whether the increase in dynamics we observed was in the P-loop and/or in the structured β-sheet comprising Src's N-terminal lobe. Therefore, we used a chemical labeling methodology[26] to probe the dynamics of a cysteine residue (Cys280) located in the center

Please cite this article in press as: Chakraborty et al., Profiling of drug resistance in Src kinase at scale uncovers a regulatory network coupling autoinhibition and catalytic domain dynamics, Cell Chemical Biology (2023), https://doi.org/10.1016/j.chembiol.2023.08.005

of Src's P-loop. Specifically, we compared the rates of N-ethylmaleimide (NEM) labeling of Cys280 in WT Src^{CD} and W285T Src^{CD}. Consistent with the notion that activating mutations in the β1/β2 resistance cluster modulate the dynamics of Src's P-loop, Cys280 in W285T Src^{CD} showed a significantly increased rate of NEM labeling relative to WT Src^{CD} (Figure 6E). Thus, activating mutations in the β1/β2 resistance cluster not only increase the overall dynamics of the catalytic domain's N-terminal lobe but also increase the dynamics of the P-loop. We speculate that residues in the β1/β2 resistance cluster act as a network that couples the dynamics of the P-loop to autoinhibitory SH2/SH3 domain interactions that occur on the opposite face of Src's catalytic domain.

DISCUSSION

Here, we leveraged a yeast-based assay to profile drug resistance in Src. We found that mutations at many residues that the line the ATP-binding pocket of Src's catalytic domain were capable of conferring resistance to inhibition. Our results with a matched panel of conformation-selective, ATP-competitive inhibitors highlight that many sites within the ATP-binding site where drug resistance occurs are inhibitor independent but that the conformational rearrangements required for certain modes of ATP-competitive inhibition raises opportunities for the emergence of unique mechanisms of resistance. Despite the large number of resistance mutations that line the ATP-binding site of Src, inhibitor contact residues did not represent the most general sites of resistance. Instead, residues that participate in Src's autoinhibition were particularly prone to the development of resistance and mutations that both reduced inhibitor affinity and increased Src's phosphotransferase activity provided the strongest levels of resistance.

Numerous mutations in a cluster of six residues (β1/β2 resistance cluster) located on the solvent-exposed face of the N-terminal lobe of Src's catalytic domain were capable of conferring strong drug resistance. The ability of mutations within the β1/β2 resistance cluster to both diminish inhibitor affinity and increase Src's phosphotransferase activity was surprising given its location on Src's catalytic domain. Moreover, some variants in this cluster that increase phosphotransferase activity also increase dependence on Hsp90 by promoting an open conformation.[33] The sidechains of all but one (Leu276) of the six residues in β1/β2 resistance cluster are directed away from Src's ATP-binding site and the top face of Src's N-terminal lobe has not previously been characterized as a regulatory interface. We found that residues within the β1/β2 resistance cluster appear to be required for limiting the conformational dynamics of Src's N-terminal lobe and that mutations at these residues release the autoinhibitory interactions required to downregulate Src's phosphotransferase activity. Thus, residues within the β1/β2 resistance cluster act as a network that couples regulatory domain engagement to the conformational rearrangements in the catalytic domain required for autoinhibition. Mutations that decrease inhibitor residence time by increasing dynamics have been identified as a pathway of resistance in the closely related tyrosine kinase Abl,[23,34] and it is likely that mutations in the β1/β2 resistance cluster could have a similar effect. Furthermore, our biochemical analyses suggest that the β1/β2 resistance cluster also modulates the dynamics of Src's P-loop. Residues within the P-loop of Abl are major sites of resistance to inhibitors of the oncogenic fusion protein BCR-Abl in the clinic (Figures S5C and S5D).[35,36] However, we observed very few inhibitor resistance mutations in Src's P-loop because almost all substitutions at these residues were found to be inactivating in our yeast growth assay (Figure S5E), which is consistent with previously observed differences in the dynamics between the P-loops of Src and Abl.[37] Thus, the ability of activating β1/β2 resistance cluster mutations to modulate the conformation of Src's P-loop while enhancing its phosphotransferase activity may provide a route for acquiring drug resistance that does not require mutation of the P-loop itself. Together, our studies highlight the insights into kinase dynamics and regulation that can be obtained by performing systematic analyses of drug resistance.

Limitations of the study

While we were able to provide additional insight into potential mechanisms of drug resistance in protein kinases, our study is limited in several ways. We screened a panel of inhibitors that stabilize different conformations of Src's ATP-binding site, but all of these inhibitors target multiple tyrosine kinases beyond Src and Src-family kinases. Thus, we are not able to provide molecular insight into how resistance can be obtained to inhibitors that target unique structural features within a kinase that confer high selectivity within the kinome. We performed inhibitor resistance profiling in yeast, which lack the extrinsic factors present in mammalian cells that regulate Src's phosphotransferase activity. While the absence of these factors simplifies the mechanistic interpretation of inhibitor resistance, the overall level of resistance a specific mutation provides in mammalian cells may not always correlate. Follow up studies in mammalian cells will be needed to determine the physiological relevance of specific resistance mutations.

SIGNIFICANCE

Proteins kinases have demonstrated a remarkable ability to acquire mutations that render them less susceptible to inhibition by ATP-competitive inhibitors. Despite the cataloging of numerous resistance mutations with model studies and in the clinic, a comprehensive understanding of the mechanistic basis of kinase drug resistance is still lacking. To gain a greater understanding of drug resistance in a multidomain protein kinase, we used a yeast-based screen to determine how almost every mutation in Src's catalytic domain affects its ability to be inhibited by ATP-competitive inhibitors. Using our yeast-based assay, we compared how mutations affect Src's phosphotransferase activity in the absence of inhibitors with its activity in the presence of various ATP-competitive inhibitors. As expected, we observed that most inhibitor resistance mutations had a WT-like or activating effect on Src's phosphotransferase activity in the absence of inhibitors. We also found that a number of mutations at positions that the line the ATP-binding site of Src provided general resistance to ATP-competitive inhibitors. However, a subset of resistance mutations appear to be specific to the structural rearrangements required for certain modes of ATP-competitive inhibition.

While inhibitor contact residues represented sites of resistance, we found that residues that participate in the autoinhibition of Src are particularly prone to the development of resistance. Biochemical analysis of a resistance-prone cluster of residues revealed that the top face of Src catalytic domain's N-terminal lobe, unexpectedly, contributes to the autoinhibition of Src and that mutations in this region led to resistance by lowering inhibitor affinity and promoting kinase hyperactivation. Together, our studies demonstrate how comprehensive profiling of drug resistance can be used to understand potential resistance pathways and uncover new mechanisms of kinase regulation.

STAR★METHODS

Detailed methods are provided in the online version of this paper and include the following:

- KEY RESOURCES TABLE
- RESOURCE AVAILABILITY
  - Lead contact
  - Materials availability
  - Data and code availability
- EXPERIMENTAL MODEL AND STUDY PARTICIPANT DETAILS
  - *S. cerevisiae* genetics and cell culture
  - Bacterial cell culture
- METHOD DETAILS
  - Cloning
  - Western blotting
  - Thermo-competent *E.Coli* (BL21 DE3) cells expressing YopH and GroEL
  - Protein purification and expression
  - *In vitro* assays of Src variant's phosphotransferase activity
  - *In vitro* assays of Src variant's K_M [ATP]
  - *In vitro* assays of Src variant's IC_{50} and K_i values
  - SFK yeast growth assay
  - Creation of Src catalytic domain mutant library
  - Subassembly of Src variant library
  - Src library transformation into yeast
  - Inhibitor screening of Src variant library
  - Calculation of Src variant activity scores
  - Identifying resistance mutations
  - SH3 domain pulldown assays
  - Limited proteolysis of Src with thermolysin
  - HDX-MS of Src
  - Maleimide labeling and mass spectrometry
  - Synthesis of inhibitors
  - Synthesis of 3-(4-amino-1-cyclopentyl-1*H*-pyrazolo[3,4-*d*ay]pyrimidin-3-yl)phenol (inhibitor **1**)
  - Synthesis of 1-cyclopentyl-3-(4-phenoxyphenyl)-1*H*-pyrazolo[3,4-*d*ay]pyrimidin-4-amine (inhibitor **2**)
  - Synthesis of *N*-(3-ethynyl-4-methylphenyl)-3-(trifluoromethyl)benzamide
  - Synthesis of *N*-(3-((4-amino-1-cyclopentyl-1*H*-pyrazolo[3,4-*d*ay]pyrimidin-3-yl)ethynyl)-4-methylphenyl)-3-(trifluoromethyl)benzamide (inhibitor **3**)
  - Synthesis of *N*-(3-((4-amino-1-methyl-1*H*-pyrazolo[3,4-*d*ay]pyrimidin-3-yl)ethynyl)-4-methylphenyl)-3-(trifluoromethyl)benzamide (inhibitor **4**)
- QUANTIFICATION AND STATISTICAL ANALYSIS
  - Calculation of K_I, IC_{50} and K_M
  - Calculation of Src phosphotransferase activity

SUPPLEMENTAL INFORMATION

Supplemental information can be found online at https://doi.org/10.1016/j.chembiol.2023.08.005.

ACKNOWLEDGMENTS

This work was supported by the National Institute of General Medical Sciences (R01GM109110 to D.M.F. and R01GM086858 to D.J.M.) and National Human Genome Research Institute (RM1HG010461 to D.M.F).

AUTHOR CONTRIBUTIONS

Conceptualization, S.C., E.A., D.M.F., and D.J.M.; Methodology, S.C., E.A., D.M.F., and D.J.M.; Investigation, S.C., E.A., M.G. J.J.S, L.F., Z.E.P., K.A.S., and J.J.S.; Writing – Original Draft, S.C. and D.J.M.; Writing – Review & Editing, S.C., E.A., D.M.F., and D.J.M.; Funding Acquisition, D.M.F. and D.J.M.; Resources, D.M.F. and D.J.M.; Supervision, D.M.F. and D.J.M.

DECLARATION OF INTERESTS

Authors declare no competing interests.

INCLUSION AND DIVERSITY

We support inclusive, diverse, and equitable conduct of research.

Received: March 19, 2023
Revised: July 3, 2023
Accepted: August 16, 2023
Published: September 7, 2023

REFERENCES

1. Gharwan, H., and Groninger, H. (2016). Kinase inhibitors and monoclonal antibodies in oncology: clinical implications. Nat. Rev. Clin. Oncol. *13*, 209–227. https://doi.org/10.1038/nrclinonc.2015.213.
2. Zhang, J., Yang, P.L., and Gray, N.S. (2009). Targeting cancer with small molecule kinase inhibitors. Nat. Rev. Cancer *9*, 28–39. https://doi.org/10.1038/nrc2559.
3. Cohen, P., Cross, D., and Jänne, P.A. (2021). Kinase drug discovery 20 years after imatinib: progress and future directions. Nat. Rev. Drug Discov. *20*, 551–569. https://doi.org/10.1038/s41573-021-00195-4.
4. Garraway, L.A., and Jänne, P.A. (2012). Circumventing cancer drug resistance in the era of personalized medicine. Cancer Discov. *2*, 214–226. https://doi.org/10.1158/2159-8290.CD-12-0012.
5. Lovly, C.M., and Shaw, A.T. (2014). Molecular pathways: resistance to kinase inhibitors and implications for therapeutic strategies. Clin. Cancer Res. *20*, 2249–2256. https://doi.org/10.1158/1078-0432.CCR-13-1610.
6. Krishnamurty, R., and Maly, D.J. (2010). Biochemical mechanisms of resistance to small-molecule protein kinase inhibitors. ACS Chem. Biol. *5*, 121–138. https://doi.org/10.1021/cb9002656.
7. Gibbons, D.L., Pricl, S., Kantarjian, H., Cortes, J., and Quintás-Cardama, A. (2012). The rise and fall of gatekeeper mutations? The BCR-ABL1 T315I paradigm. Cancer *118*, 293–299. https://doi.org/10.1002/cncr.26225.
8. Patel, R.K., Patel, Y.K., and Smithgall, T.E. (2020). Evolution Reveals a Single Mutation as Sole Source of Src-Family Kinase C-Helix-out Inhibitor Resistance. ACS Chem. Biol. *15*, 2175–2184. https://doi.org/10.1021/acschembio.0c00373.

9. Balzano, D., Santaguida, S., Musacchio, A., and Villa, F. (2011). A general framework for inhibitor resistance in protein kinases. Chem. Biol. *18*, 966–975. https://doi.org/10.1016/j.chembiol.2011.04.013.

10. Yun, C.H., Mengwasser, K.E., Toms, A.V., Woo, M.S., Greulich, H., Wong, K.K., Meyerson, M., and Eck, M.J. (2008). The T790M mutation in EGFR kinase causes drug resistance by increasing the affinity for ATP. Proc. Natl. Acad. Sci. USA *105*, 2070–2075. https://doi.org/10.1073/pnas.0709662105.

11. Azam, M., Seeliger, M.A., Gray, N.S., Kuriyan, J., and Daley, G.Q. (2008). Activation of tyrosine kinases by mutation of the gatekeeper threonine. Nat. Struct. Mol. Biol. *15*, 1109–1118. https://doi.org/10.1038/nsmb.1486.

12. Fowler, D.M., and Fields, S. (2014). Deep mutational scanning: a new style of protein science. Nat. Methods *11*, 801–807. https://doi.org/10.1038/nmeth.3027.

13. Fowler, D.M., Araya, C.L., Fleishman, S.J., Kellogg, E.H., Stephany, J.J., Baker, D., and Fields, S. (2010). High-resolution mapping of protein sequence-function relationships. Nat. Methods *7*, 741–746. https://doi.org/10.1038/nmeth.1492.

14. Ahler, E., Register, A.C., Chakraborty, S., Fang, L., Dieter, E.M., Sitko, K.A., Vidadala, R.S.R., Trevillian, B.M., Golkowski, M., Gelman, H., et al. (2019). A Combined Approach Reveals a Regulatory Mechanism Coupling Src's Kinase Activity, Localization, and Phosphotransferase-Independent Functions. Mol. Cell *74*, 393–408.e20. https://doi.org/10.1016/j.molcel.2019.02.003.

15. Brugge, J.S., Jarosik, G., Andersen, J., Queral-Lustig, A., Fedor-Chaiken, M., and Broach, J.R. (1987). Expression of Rous sarcoma virus transforming protein pp60v-src in Saccharomyces cerevisiae cells. Mol. Cell Biol. *7*, 2180–2187. https://doi.org/10.1128/mcb.7.6.2180-2187.1987.

16. Kritzer, J.A., Freyzon, Y., and Lindquist, S. (2018). Yeast can accommodate phosphotyrosine: v-Src toxicity in yeast arises from a single disrupted pathway. FEMS Yeast Res. *18*, foy027. https://doi.org/10.1093/femsyr/foy027.

17. Jain, P.C., and Varadarajan, R. (2014). A rapid, efficient, and economical inverse polymerase chain reaction-based method for generating a site saturation mutant library. Anal. Biochem. *449*, 90–98. https://doi.org/10.1016/j.ab.2013.12.002.

18. Hiatt, J.B., Patwardhan, R.P., Turner, E.H., Lee, C., and Shendure, J. (2010). Parallel, tag-directed assembly of locally derived short sequence reads. Nat. Methods *7*, 119–122. https://doi.org/10.1038/nmeth.1416.

19. Hiatt, J.B., Pritchard, C.C., Salipante, S.J., O'Roak, B.J., and Shendure, J. (2013). Single molecule molecular inversion probes for targeted, high-accuracy detection of low-frequency variation. Genome Res. *23*, 843–854. https://doi.org/10.1101/gr.147686.112.

20. Starita, L.M., and Fields, S. (2015). Deep Mutational Scanning: Library Construction, Functional Selection, and High-Throughput Sequencing. Cold Spring Harb. Protoc. *2015*, 777–780. https://doi.org/10.1101/pdb.prot085225.

21. Rubin, A.F., Gelman, H., Lucas, N., Bajjalieh, S.M., Papenfuss, A.T., Speed, T.P., and Fowler, D.M. (2017). A statistical framework for analyzing deep mutational scanning data. Genome Biol. *18*, 150. https://doi.org/10.1186/s13059-017-1272-5.

22. Persky, N.S., Hernandez, D., Do Carmo, M., Brenan, L., Cohen, O., Kitajima, S., Nayar, U., Walker, A., Pantel, S., Lee, Y., et al. (2020). Defining the landscape of ATP-competitive inhibitor resistance residues in protein kinases. Nat. Struct. Mol. Biol. *27*, 92–104. https://doi.org/10.1038/s41594-019-0358-z.

23. Lyczek, A., Berger, B.T., Rangwala, A.M., Paung, Y., Tom, J., Philipose, H., Guo, J., Albanese, S.K., Robers, M.B., Knapp, S., et al. (2021). Mutation in Abl kinase with altered drug-binding kinetics indicates a novel mechanism of imatinib resistance. Proc. Natl. Acad. Sci. USA *118*, e2111451118. https://doi.org/10.1073/pnas.2111451118.

24. Ranjitkar, P., Brock, A.M., and Maly, D.J. (2010). Affinity reagents that target a specific inactive form of protein kinases. Chem. Biol. *17*, 195–206. https://doi.org/10.1016/j.chembiol.2010.01.008.

25. Fang, L., Vilas-Boas, J., Chakraborty, S., Potter, Z.E., Register, A.C., Seeliger, M.A., and Maly, D.J. (2020). How ATP-Competitive Inhibitors Allosterically Modulate Tyrosine Kinases That Contain a Src-like Regulatory Architecture. ACS Chem. Biol. *15*, 2005–2016. https://doi.org/10.1021/acschembio.0c00429.

26. Potter, Z.E., Lau, H.T., Chakraborty, S., Fang, L., Guttman, M., Ong, S.E., Fowler, D.M., and Maly, D.J. (2020). Parallel Chemoselective Profiling for Mapping Protein Structure. Cell Chem. Biol. *27*, 1084–1096.e4. https://doi.org/10.1016/j.chembiol.2020.06.014.

27. Hari, S.B., Merritt, E.A., and Maly, D.J. (2013). Sequence determinants of a specific inactive protein kinase conformation. Chem. Biol. *20*, 806–815. https://doi.org/10.1016/j.chembiol.2013.05.005.

28. Chakraborty, S., Inukai, T., Fang, L., Golkowski, M., and Maly, D.J. (2019). Targeting Dynamic ATP-Binding Site Features Allows Discrimination between Highly Homologous Protein Kinases. ACS Chem. Biol. *14*, 1249–1259. https://doi.org/10.1021/acschembio.9b00214.

29. Agius, M.P., Ko, K.S., Johnson, T.K., Kwarcinski, F.E., Phadke, S., Lachacz, E.J., and Soellner, M.B. (2019). Selective Proteolysis to Study the Global Conformation and Regulatory Mechanisms of c-Src Kinase. ACS Chem. Biol. *14*, 1556–1563. https://doi.org/10.1021/acschembio.9b00306.

30. Boczek, E.E., Luo, Q., Dehling, M., Röpke, M., Mader, S.L., Seidl, A., Kaila, V.R.I., and Buchner, J. (2019). Autophosphorylation activates c-Src kinase through global structural rearrangements. J. Biol. Chem. *294*, 13186–13197. https://doi.org/10.1074/jbc.RA119.008199.

31. Hochrein, J.M., Lerner, E.C., Schiavone, A.P., Smithgall, T.E., and Engen, J.R. (2006). An examination of dynamics crosstalk between SH2 and SH3 domains by hydrogen/deuterium exchange and mass spectrometry. Protein Sci. *15*, 65–73. https://doi.org/10.1110/ps.051782206.

32. Barouch-Bentov, R., Che, J., Lee, C.C., Yang, Y., Herman, A., Jia, Y., Velentza, A., Watson, J., Sternberg, L., Kim, S., et al. (2009). A conserved salt bridge in the G loop of multiple protein kinases is important for catalysis and for in vivo Lyn function. Mol. Cell *33*, 43–52. https://doi.org/10.1016/j.molcel.2008.12.024.

33. Nguyen, V., Ahler, E., Sitko, K.A., Stephany, J.J., Maly, D.J., and Fowler, D.M. (2023). Molecular determinants of Hsp90 dependence of Src kinase revealed by deep mutational scanning. Protein Sci. *32*, e4656. https://doi.org/10.1002/pro.4656.

34. Rangwala, A.M., Berger, B.T., Robers, M.B., Knapp, S., and Seeliger, M.A. (2022). Resistance to kinase inhibition through shortened target engagement. Mol. Cell. Oncol. *9*, 2029999. https://doi.org/10.1080/23723556.2022.2029999.

35. Redaelli, S., Piazza, R., Rostagno, R., Magistroni, V., Perini, P., Marega, M., Gambacorti-Passerini, C., and Boschelli, F. (2009). Activity of bosutinib, dasatinib, and nilotinib against 18 imatinib-resistant BCR/ABL mutants. J. Clin. Oncol. *27*, 469–471. https://doi.org/10.1200/JCO.2008.19.8853.

36. Seeliger, M.A., Ranjitkar, P., Kasap, C., Shan, Y., Shaw, D.E., Shah, N.P., Kuriyan, J., and Maly, D.J. (2009). Equally potent inhibition of c-Src and Abl by compounds that recognize inactive kinase conformations. Cancer Res. *69*, 2384–2392. https://doi.org/10.1158/0008-5472.CAN-08-3953.

37. Hari, S.B., Perera, B.G.K., Ranjitkar, P., Seeliger, M.A., and Maly, D.J. (2013). Conformation-selective inhibitors reveal differences in the activation and phosphate-binding loops of the tyrosine kinases Abl and Src. ACS Chem. Biol. *8*, 2734–2743. https://doi.org/10.1021/cb400663k.

38. Hageman, T.S., and Weis, D.D. (2019). Reliable Identification of Significant Differences in Differential Hydrogen Exchange-Mass Spectrometry Measurements Using a Hybrid Significance Testing Approach. Anal. Chem. *91*, 8008–8016. https://doi.org/10.1021/acs.analchem.9b01325.

39. Leonard, S.E., Register, A.C., Krishnamurty, R., Brighty, G.J., and Maly, D.J. (2014). Divergent modulation of Src-family kinase regulatory interactions with ATP-competitive inhibitors. ACS Chem. Biol. *9*, 1894–1905. https://doi.org/10.1021/cb500371g.

40. Wang, Q., Cahill, S.M., Blumenstein, M., and Lawrence, D.S. (2006). Self-reporting fluorescent substrates of protein tyrosine kinases. J. Am. Chem. Soc. *128*, 1808–1809. https://doi.org/10.1021/ja0577692.

41. Suzuki, Y., St Onge, R.P., Mani, R., King, O.D., Heilbut, A., Labunskyy, V.M., Chen, W., Pham, L., Zhang, L.V., Tong, A.H.Y., et al. (2011). Knocking out multigene redundancies via cycles of sexual assortment and fluorescence selection. Nat. Methods *8*, 159–164. https://doi.org/10.1038/nmeth.1550.

42. Albanese, S.K., Parton, D.L., Işık, M., Rodríguez-Laureano, L., Hanson, S.M., Behr, J.M., Gradia, S., Jeans, C., Levinson, N.M., Seeliger, M.A., and Chodera, J.D. (2018). An Open Library of Human Kinase Domain Constructs for Automated Bacterial Expression. Biochemistry *57*, 4675–4689. https://doi.org/10.1021/acs.biochem.7b01081.

43. Gietz, R.D., and Schiestl, R.H. (2007). High-efficiency yeast transformation using the LiAc/SS carrier DNA/PEG method. Nat. Protoc. *2*, 31–34. https://doi.org/10.1038/nprot.2007.13.

44. García-Nafría, J., Watson, J.F., and Greger, I.H. (2016). IVA cloning: A single-tube universal cloning system exploiting bacterial In Vivo Assembly. Sci. Rep. *6*, 27459. https://doi.org/10.1038/srep27459.

45. Wang, L., Pan, H., and Smith, D.L. (2002). Hydrogen exchange-mass spectrometry: optimization of digestion conditions. Mol. Cell. Proteomics *1*, 132–138. https://doi.org/10.1074/mcp.m100009-mcp200.

46. Walters, B.T., Ricciuti, A., Mayne, L., and Englander, S.W. (2012). Minimizing back exchange in the hydrogen exchange-mass spectrometry experiment. J. Am. Soc. Mass Spectrom. *23*, 2132–2139. https://doi.org/10.1007/s13361-012-0476-x.

47. Majumdar, R., Manikwar, P., Hickey, J.M., Arora, J., Middaugh, C.R., Volkin, D.B., and Weis, D.D. (2012). Minimizing carry-over in an online pepsin digestion system used for the H/D exchange mass spectrometric analysis of an IgG1 monoclonal antibody. J. Am. Soc. Mass Spectrom. *23*, 2140–2148. https://doi.org/10.1007/s13361-012-0485-9.

48. Hamuro, Y., and Coales, S.J. (2018). Optimization of Feasibility Stage for Hydrogen/Deuterium Exchange Mass Spectrometry. J. Am. Soc. Mass Spectrom. *29*, 623–629. https://doi.org/10.1007/s13361-017-1860-3.

49. Fang, J., Rand, K.D., Beuning, P.J., and Engen, J.R. (2011). False EX1 signatures caused by sample carryover during HX MS analyses. Int. J. Mass Spectrom. *302*, 19–25. https://doi.org/10.1016/j.ijms.2010.06.039.

50. Baker, P.R., and Chalkley, R.J. (2014). MS-viewer: a web-based spectral viewer for proteomics results. Mol. Cell. Proteomics *13*, 1392–1396. https://doi.org/10.1074/mcp.O113.037200.

51. Zhang, Z., Zhang, A., and Xiao, G. (2012). Improved protein hydrogen/deuterium exchange mass spectrometry platform with fully automated data processing. Anal. Chem. *84*, 4942–4949. https://doi.org/10.1021/ac300535r.

52. Kahsai, A.W., Rajagopal, S., Sun, J., and Xiao, K. (2014). Monitoring protein conformational changes and dynamics using stable-isotope labeling and mass spectrometry. Nat. Protoc. *9*, 1301–1319. https://doi.org/10.1038/nprot.2014.075.

53. Lamppa, J.W., and Tanyos, S.A. (2013). Engineering Escherichia coli for soluble expression and single-step purification of active human lysozyme. J. Biotechnol. *164*, 1–8. https://doi.org/10.1016/j.jbiotec.2012.11.007.

Please cite this article in press as: Chakraborty et al., Profiling of drug resistance in Src kinase at scale uncovers a regulatory network coupling auto-inhibition and catalytic domain dynamics, Cell Chemical Biology (2023), https://doi.org/10.1016/j.chembiol.2023.08.005

CellPress

STAR★METHODS

KEY RESOURCES TABLE

REAGENT or RESOURCE	SOURCE	IDENTIFIER
Antibodies		
Rabbit monoclonal anti-Src (36D10)	Cell Signaling	Cat#2109; RRID: AB_2106059
Mouse monoclonal anti-non- phospho (Y416)	Cell Signaling	Cat#2102; RRID: AB_331358
Bacterial and virus strains		
E. coli (BL21 DE3 +GroEL + YopH)	This paper	N/A
NEB 5-alpha Competent *E. coli* (high efficiency)	New England Biolabs	Cat# C2987H
NEB BL21(DE3) Competent *E. coli*	New England Biolabs	Cat# C2527H
Chemicals, peptides, and recombinant proteins		
SNAPtag-VSLARRPLPPLP	Leonard et al.[39]	N/A
SFK peptide (EEEIYGE-(DAP- Pyrene)-EA)	Wang et al.[40]	N/A
Inhibitor **1**	Fang et al.[25]	N/A
Inhibitor **2**	Ahler et al.[14]	N/A
Inhibitor **3**	Ahler et al.[14]	N/A
Inhibitor **4**	This paper	N/A
Dasatinib	SelleckChem	Cat# S1021
2-Mercaptoethanol	BIO-RAD	Cat# 1610710
Potassium Acetate (KOAc)	Invitrogen	Cat# AM9610
Calcium Chloride ($CaCl_2$)	Thermo Fisher Scientific	Cat# 012316-A7
Manganese Chloride ($MnCl_2$)	Thermo Fisher Scientific	Cat# 011868.36
Magnesium Chloride ($MgCl_2$)	Thermo Fisher Scientific	Cat# AB0359
Glycerol	Thermo Fisher Scientific	Cat# A16205-AP
Isopropyl β-D-1-thiogalactopyranoside (IPTG)	Invitrogen	Cat# 15529019
Ampicillin	Gibco	Cat# 11593027
Streptomycin	Gibco	Cat# 11860038
Chloramphenicol	Thermo Fisher Scientific	Cat# B20841.14
Pierce retention time calibration mix	Thermo Fisher Scientific	Cat# 88321
Thermolysin	Promega	Cat# V4001
Glu-1-Fibrino (GluFib) peptide CAS#103213-49-6	Sigma	Cat# F3261-.1MG
NHS-sepharose beads Fast-flow (4B)	Millipore Sigma	Cat# GE17-0906-01
SYPRO Ruby staining solution	BIO-RAD	Cat# 1703125
Pierce MS Grade Trypsin	Thermo Fisher Scientific	Cat# PI90057
Pierce N-ethylmaleimide	Thermo Fisher Scientific	Cat# 23030
Thin walled PCR tubes	Fisher Scientific	Cat# 14230200
Deuterated water (D_2O)	Cambridge Isotope labs	Cat# DLM-6-10X1
Glass vials	Waters	Cat# 186002805
Chemicals, peptides, and recombinant proteins		
Magnetic caps	PalParts	Cat# LAP.09151907
Trap column cartridge	Waters	Cat# 186007817
C-18 column	Waters	Cat# 186006934
Optima grade LC-MS water	Fisher Scientific	Cat# W6-4
Src^{FL} (WT, E283M, V326K, or W285T)	This paper	N/A
Src^{3D} (WT, W285T, E283M, or E283D)	This paper	N/A
Src^{CD} (WT, W285T, E283M, or E283D)	This paper	N/A
Src^{EEI} (WT,W285T, or E283M)	This paper	N/A
His_6-ULP1	This paper	N/A

(*Continued on next page*)

Please cite this article in press as: Chakraborty et al., Profiling of drug resistance in Src kinase at scale uncovers a regulatory network coupling auto-inhibition and catalytic domain dynamics, Cell Chemical Biology (2023), https://doi.org/10.1016/j.chembiol.2023.08.005

Continued

REAGENT or RESOURCE	SOURCE	IDENTIFIER
Critical commercial assays		
Library Quantification Kit (Illumina)	KAPA Biosystems	Cat# KK4854
LB Broth Miller	Thermo Fisher Scientific	Cat# 611875000
Terrific Broth	Invitrogen	Cat# 22711022
SOC outgrowth medium	New England Biolabs	Cat# B9020S
MiSeq Reagent Kit v2 (300 cycles)	Illumina	Cat# MS-102-2002
NextSeq 500/550 High Output v2 kit (75 cycles)	Illumina	Cat# FC-404-2005
Zeba Spin Desalting Column	Thermo	Cat# 89882
Yeast Plasmid Prep Kit I	Zymo Research	Cat# D2001
DNA Clean & Concentrator	Zymo Research	Cat# D4004
QIAGEN Plasmid Midi Kit	QIAGEN	Cat#12143
Deposited data		
Github Repository	This paper	Github: https://github.com/eahler/2023_src_inhib
Raw and analyzed data: Sequencing reads	This paper	GEO: GSE190495
Experimental models: Organisms/strains		
S. cerevisiae. Strain Background: "Green Monster"	Frederick P. Roth Lab (Suzuki et al.)[41]	N/A
S. cerevisiae. BY4741 ΔPDR5	Stanley Fields Lab	N/A
Oligonucleotides		
DNA Oligos	This paper	See Table S2 for list of all oligonucleotides used in this study
Recombinant DNA		
p415 GAL1	ATCC	Cat# 87330
pMCSG7	Novopro	Cat# V010607
pET13SA-YopH	Albanese et al.[42]	Addgene Cat# 79749
pACYC-GroEL	Lamppa et al. [53]	Addgene Cat# 83923
pMCSG7-His_6-SUMO-Src^{FL} (WT, E283M, V326K, or W285T)	This Paper	N/A
pMCSG7-His_6-SUMO-Src^{3D} (WT, W285T, E283M, or E283D)	This Paper	N/A
pMCSG7-His_6-SUMO-Src^{CD} (WT, W285T, E283M, or E283D)	This Paper	N/A
pMCSG7-His_6-SUMO-Src^{EEI} (WT or W285T)	This Paper	N/A
pMCSG7-His_6-ULP1	This Paper	N/A
Software and algorithms		
PyMOL v1.10	Schrödinger	Pymol: https://pymol.org/
Enrich2	Rubin et al.[21]	Github: https://github.com/FowlerLab/Enrich2
ImageJ v1.44	National Institutes of Health	Image J: https://imagej.nih.gov/ij
RStudio v4.3.1	Posit, PBC	Rstudio: https://cran.r-project.org/
GraphPad Prism 8.2.4	GraphPad	GraphPad: https://www.graphpad.com/scientific-software/prism/
HD-Examiner 2.4	Sierra Analytics	HD-Examiner: http://massspec.com/hdexaminer/
Image Studio Lite	LI-COR Biosciences	Image Studio Lite: https://www.licor.com/bio/products/software/image_studio_lite/
Xcalibur Data Acquisition and analysis	Thermo Fisher Scientific	Xcalibur: http://www.coxdocs.org/doku.php?id=perseus:start

Please cite this article in press as: Chakraborty et al., Profiling of drug resistance in Src kinase at scale uncovers a regulatory network coupling auto-inhibition and catalytic domain dynamics, Cell Chemical Biology (2023), https://doi.org/10.1016/j.chembiol.2023.08.005

CellPress

RESOURCE AVAILABILITY

Lead contact

Further information and requests for resources and reagents should be directed to and will be fulfilled by the Lead Contact, Dustin J. Maly (djmaly@uw.edu).

Materials availability

All unique/stable reagents generated in this study are available from the lead contact without restriction.

Data and code availability

- Accession numbers and links to all python and R code Sequencing reads were deposited in NCBI's Gene Expression Omnibus (GEO) and are accessible through accession number GSE190495. Raw Data for the Src DMS and code to reproduce figures are located in our Github repository at: https://github.com/eahler/2023_src_inhib.
- This paper does not report original code.
- Any additional information required to reanalyze the data reported in this paper is available from the lead contact upon request

EXPERIMENTAL MODEL AND STUDY PARTICIPANT DETAILS

S. cerevisiae genetics and cell culture

BY4741 Green Monster (a generous gift from Dr. Fritz Roth, inhibitors **1**, **2** and **4**)[41] or BY4741 (ΔPDR5, MATa His3D1 Leu2D0 Met15D0 Ura3D0, dasatinib) were used to perform yeast experiments. All Src^{myr} and Lyn^{myr} constructs were cloned into the p415 GAL1 plasmid. To select successful transformants, yeast was transformed using standard LiAc protocols[43] and plated on C-Leu media. All growth experiments were performed in C-Leu media to maintain plasmid.

Bacterial cell culture

In vitro experiments were performed with recombinant protein purified from thermo-competent *E.Coli* (BL21 DE3) cells expressing YopH and GroEL.

METHOD DETAILS

Restriction enzymes were purchased from New England Biolabs and all chemicals purchased from Sigma unless otherwise specified.

Cloning

QuickChange Site Directed Mutagenesis (Agilent) or IVA cloning[44] was used to generate all mutants discussed in the paper following standard protocols. Mutations were verified by Sanger sequencing of the entire open reading frame. Gibson assembly or directional cloning following standard protocols was performed to achieve all subcloning and all constructs were validated by Sanger sequencing.

Western blotting

Src antibody (36D10; CST #2109) and Non-phospho-Src (Tyr416) (7G9; CST #2102) were purchased from Cell Signaling Technology (CST). Anti-rabbit secondary antibody was purchased from Li-Cor.

Thermo-competent *E.Coli* (BL21 DE3) cells expressing YopH and GroEL

pET13SA-YopH[42] and pACYC-GroEL[53] were co-transformed into NEB BL21(DE3) competent *E. coli* and plated on dual selective LB agar plates (Spectromycin 50 μg/mL (pET13SA-YopH)) and Chloramphenicol 25 μg/mL (pACYC-GroEL)). A single colony was picked the next day and grown overnight in 5 mL of LB broth miller with Spectromycin (50 μg/mL) and Chloramphenicol (25 μg/mL). The following day, 125 mL of SOC outgrowth medium with Spectromycin (50 μg/mL) and Chloramphenicol (25 μg/mL) was inoculated with the entire 5 mL of seed culture, and the culture was shaken at 37°C until the culture reached an $O.D._{600}$ of 0.3. Next, the culture flask was plunged into an ice bath, and cooled for 10 min. Next, the culture was dispensed into pre-chilled Falcon tubes and pelleted at 4°C at 2800 xg for 10 min. The supernatant was discarded, and the cell pellet was resuspended into 10 mL of pre-chilled cell culture buffer (10 mM KOAc, 80 mM $CaCl_2$, 20 mM $MnCl_2$, 10 mM $MgCl_2$, 10% (v/v) glycerol, pH 6.4, sterile filtered) and aliquoted into chilled Eppendorf tubes and store at −80°C until use.

Protein purification and expression

pMCSG7-His6-ULP1 was transformed into NEB BL21(DE3) competent *E. coli* and plated on LB agar plates with 100 μg/mL Ampicillin. A single colony was picked the next day and grown overnight in 5 mL of LB broth miller containing 100 μg/mL Ampicillin. The following day, 1 L of LB broth miller containing 100 μg/mL Ampicillin was inoculated with the entire 5 mL of seed culture, and the

Please cite this article in press as: Chakraborty et al., Profiling of drug resistance in Src kinase at scale uncovers a regulatory network coupling autoinhibition and catalytic domain dynamics, Cell Chemical Biology (2023), https://doi.org/10.1016/j.chembiol.2023.08.005

culture was grown at 37°C until the culture reached an O.D.$_{600}$ of 0.6 after which the temperature was dropped to 18°C and protein expression was induced with 0.4 mM IPTG overnight. Ni-NTA was used to purify after lysing cells in lysis buffer (50 mM HEPES, pH 8.0, 300 mM NaCl, 1 mM PMSF, 0.1% Triton X-, 20 mM imidazole) and eluted using purification buffer (50 mM HEPES, pH 8.0, 300 mM NaCl, 1 mM PMSF, 0.1% Triton X-, 10% glycerol, 0.2% BME, 300 mM imidazole) to yield His$_6$-ULP1 at >95% purity. A 16 h dialysis was performed in dialysis buffer (50 mM HEPES, pH 8.0, 150 mM NaCl, 1 mM DTT, 10% glycerol) at 4°C and the purified protein was stored at −80°C until use for cleaving His$_6$-SUMO tag from various Src constructs as discussed below.

For *in vitro* biochemical assays, Src^{FL} (WT/E283M/V326K/W285T, residues 2–536), Src^{3D} (WT/W285T/E283M/E283D, residues 87–536), Src^{CD} (WT/W285T/E283M/E283D, residues 261–536) and autoinhibited Src^{EEI} (WT/W285T, residues 87–536; mutations Q531E, P532E and G533I) were cloned into the bacterial expression plasmid pMCSG7 as N-terminal His$_6$-SUMO tagged constructs. Src constructs were transformed into *E.coli* expressing YopH/GroEL and plated on triple selective plates (Ampicillin (100 μg/mL)/Chloramphenicol (25 μg/mL)/Streptomycin (50 μg/mL)). A single colony was picked and grown in an overnight culture of 15 mL of Terrific broth containing all three antibiotics. A 1 L culture was then inoculated with the starter culture, grown to an O.D.$_{600}$ of 1.1, the temperature was then dropped to 18°C and protein expression was induced with 0.4 mM IPTG overnight. Ni-NTA was used to purify His$_6$-SUMO-Src after lysing cells in lysis buffer (50 mM HEPES, pH 8.0, 300 mM NaCl, 1 mM PMSF, 0.1% Triton X-, 20 mM imidazole) and eluted using purification buffer (50 mM HEPES, pH 8.0, 300 mM NaCl, 1 mM PMSF, 0.1% Triton X-, 10% glycerol, 0.2% BME, 150 mM imidazole). A 2 h dialysis in dialysis buffer (50 mM HEPES, pH 8.0, 150 mM NaCl, 1 mM DTT, 10% glycerol) was performed at 4°C prior to adding the SUMO protease His$_6$-ULP1 (1:25 protease:eluted protein, w/w). The Src-protease mixture was then transferred to a fresh dialysis buffer and cleaved overnight at 4°C. Following cleavage, a second Ni-NTA purification was carried out to remove any non-cleaved Src and His$_6$-ULP1. Finally, an anion exchange column (Pierce, 90011) was used to remove YopH and GroEL to yield Src at > 95% purity. Relates to Figures 3D, S3G, 4B, 4D–4I, S4F–S4J, 5C, S5, 6D, and 6E.

In vitro assays of Src variant's phosphotransferase activity

Purified recombinant Src variants were used to measure Src phosphotransferase activity using a self-reporting fluorescent SFK peptide (EEEIYGE-(DAP- Pyrene)-EA)[40] in an *in vitro* kinase assay. Briefly, 20 μL of purified Src^{FL} (6.5 nM), Src^{3D} (5 nM), Src^{CD} (5.5 nM) or autoinhibited Src^{EEI} (8 nM) constructs of each variant (WT, V326K, W285T, E238M or E283D) were diluted in kinase reaction buffer (76 mM HEPES, pH 7.5, 5 mM $MgCl_2$, 150 mM NaCl, 3.8 mM EGTA, 0.2 mg/mL BSA, 150 μM Sodium orthovanadate (Na_3VO_4)) and incubated with 5 μL of 5 mM ATP at room temperature for 30 min. Next, 5 μL of 200 μM SFK peptide was added to each well and raw fluorescence units were measured immediately on an Envision fluorometer (PerkinElmer) with an excitation wavelength of 344 nm and an emission wavelength of 405 nm in real time for the first 15 min at 15 s intervals. Calculation of kinase activity in terms of pmole s^{-1} of phosphorylated substrate per nM of enzyme is discussed below under "Calculation of Src activity." Relates to Figures S3G, 4D–4F, and 6D.

In vitro assays of Src variant's K_M [ATP]

K_M [ATP] of purified Src variants were measured using the same assay described above. Briefly, 2-fold (8-data points) serial dilution of ATP starting at 1 mM, was incubated with 5 nM of Src (WT or mutant) in kinase reaction buffer (76 mM HEPES, pH 7.5, 5 mM $MgCl_2$, 150 mM NaCl, 3.8 mM EGTA, 0.2 mg/mL BSA, 150 μM Na_3VO_4) and 20 μM of SFK peptide. Raw fluorescence units were measured immediately on an Envision fluorometer (PerkinElmer) with an excitation wavelength of 344 nm and an emission wavelength of 405 nm in real time for 90 min at 15 min intervals. Calculation of kinase Km [ATP] is discussed below under "Calculation of IC_{50}, K_M, K_I." Relates to Figures S3G and S4G.

In vitro assays of Src variant's IC_{50} and K_i values

For all IC_{50} determination experiments, first a kinase titration was performed as described above prior to inhibitor titration to ensure linearity of kinase concentration in the assay.

Inhibitors (initial concentration = 30 μM, 3-fold serial dilutions, 10 data points in triplicate) were assayed against Src^{FL} ([WT] = 4 nM; [W285T] = 5 nM; [V326K] = 5 nM; [E283M] = 4.5 nM), and Src^{CD} ([WT] = 3.5 nM, [W285T] = 5 nM; [E283M] = 4.5 nM) in assay buffer (76 mM HEPES, pH 7.5, 5 mM $MgCl_2$, 150 mM NaCl, 3.8 mM EGTA, 0.2 mg/mL BSA, 150 μM Na_3VO_4). Briefly, kinase was pre-incubated with 1 mM ATP and inhibitors for 30 min in a 384-black assay plate (Corning, #3573). 20 μM of SFK peptide was then added to plate and incubated for 2 h. Raw fluorescence units were measured on Envision (PerkinElmer) with excitation wavelength of 344 nm and emission wavelength of 405 nm. Data were analyzed using GraphPad Prism 8.4.2 software, IC_{50} determination and K_I calculation are discussed below under "Calculation of IC_{50}, K_M, K_I." Relates to Figures 3D and 4B.

SFK yeast growth assay

SFK yeast growth assay was performed as previously described.[14] Briefly, codon-optimized full-length human Src or Lyn (WT or indicated mutants) were transformed into the *S. cerevisiae* BY4741 Green Monster using standard LiAc transformation protocols[43] and plated on C-Leu plates to select for successful transformants. Two or three independent colonies for each strain were collected and treated as biological replicates. Single colonies for each strain were grown overnight in 5 mL of 3% raffinose C-Leu to saturation. The following day cultures were back diluted to O.D.$_{600}$ = 0.5 in C-Leu 3% raffinose and grown to at least O.D.$_{600}$ = 1.0 before subsequent dilution. To induce expression, cultures were diluted to O.D.$_{600}$ = 0.01 into C-Leu 2% galactose, then 150 μL of each culture was plated and grown in a BioTek Synergy plate reader under constant shaking at 30°C. O.D$_{600}$ was measured every 30 min over a 36 or 48 h period.

Please cite this article in press as: Chakraborty et al., Profiling of drug resistance in Src kinase at scale uncovers a regulatory network coupling autoinhibition and catalytic domain dynamics, Cell Chemical Biology (2023), https://doi.org/10.1016/j.chembiol.2023.08.005

For SFK yeast growth assays with inhibitors, the same procedures were followed as above except the indicated inhibitor concentration (or DMSO vehicle control) was added at the time of induction (final DMSO = 1%).

To calculate the growth rate for an individual variant, background corrected $O.D._{600}$ values within the range 0.04–0.32 from the yeast growth assay, corresponding to 2–5 doublings, were used. During this phase of growth, the effects of culture density and detector signal sensitivity on yeast growth rate were negligible, ensuring a linear growth pattern. The background-corrected $O.D._{600}$ values were natural log-transformed and the slope of the line for time vs. $\ln(O.D._{600})$ were calculated (reported as the growth rate). Relates to Figures S1,S5A, and 6C.

Creation of Src catalytic domain mutant library

An inverse PCR saturation mutagenesis strategy[17] was used to create the Src variant library.[14] Primer pairs corresponding to each of the 250 positions of Src's catalytic domain (residues 270–519) in p415 GAL1 Src (primer sequences located in Table S2) were generated. At every mutagenized position, the forward primer contained a degenerate 'NNK' codon (''N'' = any possible nucleotide, ''K'' = ''G'' or ''T''). Paired reverse primers were designed to sit directly upstream of the NNK-containing forward primers. Primer pairs (ordered in 96-well format (Integrated DNA Technologies)) were matched for their melting temperature and GC content. 2 μL of a mixture of forward (2.5 μM) and reverse (2.5 μM) primers for each mutagenized position, 1 μL of 500 pg/mL p415 GAL1 Src, 10 μL of 2x KAPA HiFI HotStart ReadyMix (KAPA Biosystems), and 5 μL H_2O were used to amplify each position (thermocycler conditions = an initial cycle of 95°C for 3 min, followed by 20 cycles of 98°C for 20 s, 60°C for 15 s, and 72°C for 8.5 min, and a final cycle at 72°C for 10 min). ~90% of all positions were amplified using the aforementioned thermocycler conditions. For the remaining positions that were not successfully amplified, optimized thermocycler conditions were determined. To verify that expected amplifications were obtained, 5 μL of each reaction was run on an agarose gel, and band intensities were quantified (ImageJ: (https://imagej.nih.gov/ij)) using a standard curve. Measured intensities at each position were used for binning and pooling, and the pooled library was 5' phosphorylated with T4 Polynucleotide Kinase (37°C for 30 min, followed by a heat inactivation step at 65°C for 20 min). The 5′ phosphorylated products were then ligated with T4 DNA Ligase at 16°C overnight, cleaned, and transformed into One Shot TOP10F Electrocomp *E. coli* (Thermo Fisher) using electroporation. To ascertain library size, transformed cells were plated on LB + Ampicillin plates, inoculated into LB + Ampicillin liquid, and prepped using GenElute Midiprep Kit (Sigma).

Subassembly of Src variant library

A modification of a previously described method[18] was used for subassembly of the Src variant library. A double-stranded version of SC01 barcodes (primer sequences located in Table S2) was generated by mixing 4.5 μL of the SC01 primer mixture (25 μM), 4.5 μL of the SC02 primer (25 μM), 4 μL of Buffer 3.1, and 27 μL H_2O, which was heated at 98°C for 3 min, and then ramped down to 25°C at a rate of 0.1 °C/s. 1 μL of DNA Polymerase I (Large Fragment, New England Biolabs) and 1.35 μL of 1mM dNTPS (QIAGEN) were then added to this mixture and incubated at 25°C for 15 min. Double-stranded SC01 barcodes were then cleaned using DNA clean and concentrator (Zymo Research) and eluted with 10 μL of H_2O. 10 μL of the Src variant library in p415 GAL1 Src (268 ng/mL) was digested overnight at 37°C with 1 μL SalI-HF in 5 μL 10x Cutsmart Buffer and 34 μL of H_2O. The digested Src variant library in p415 GAL1 Src was then incubated for 1 h at 37°C with a mixture of 5 μL 10x Antarctic Phosphatase Buffer and 1 μL Antarctic Phosphatase, followed by heat inactivation for 5 min at 70°C and gel extraction (QIAGEN), which was then cleaned and eluted in 10 μL of H_2O. A mixture of double-stranded SC01 barcodes (150 ng) and the digested Src variant library in p415 GAL1 Src (100 ng) was incubated for 1 h at 50°C in 2x Gibson Mastermix, and then cleaned and transformed into *E. coli*. To allow bottlenecking at the desired library size, multiple Gibson reactions were transformed in parallel. 100,000 colonies were selected for the Src variant library (BC Src library) that was used in all subsequent steps. Plasmid was prepared from colonies using Qiagen Midiprep Kit (Sigma). To associate barcodes with Src variants, 25 μL 2x KAPA HiFI HotStart ReadyMix, 6 μL SC03 primer (2.5 μM), 6 μL SC04 (2.5 μM), 12 μL H_2O, and 1 μL 10 ng/mL BC Src library were used to generate amplicons encompassing Src's catalytic domain and barcode (8 replicates for each of the three Bal-31 digestion conditions). The following thermocycler conditions was used: 1 cycle for 3 min at 95°C, followed by 17 cycles of 98°C for 20 s, 60°C for 15 s, and 72°C for 4.5 min. All eight replicate amplifications were pooled and cleaned. Three different Bal-31 digestion conditions (undigested, Bal-31, or ScaI/Bal-31) were used to generate fragments spanning the mutagenized region of Src's catalytic domain as follows: undigested, and Bal-31 for 30 min, and ScaI/Bal-31 digestion for 10 min. The ScaI/Bal-31 digestion was performed the following way: 20 μL of amplicon, 5 μL 10x CutSmart buffer, 24 μL H_2O, and 1 μL ScaI-HF were incubated overnight at 37°C and subsequently cleaned using DNA clean and concentrator (Zymo Research). Next, each sample was digested using Bal-31 endonuclease mixed with 25 μL of 2x Bal-31 Buffer, 40 ng/mL of amplicon, and 1 μL of 1:5 Bal-31 enzyme at 25°C for the indicated time. 10 μL of 100 mM EGTA heated to 65°C for 10 min was used to quench the digestion. All digested DNA was cleaned and run on an agarose gel to visually confirm the correct fragment range. Each digested product was treated with END-IT Kit (Epicenter), cleaned, and A-tailed by adding the entire reaction to 5 μL of 10x Taq Buffer, 8 μL H_2O, 1 μL of 10 mM ATP, and 1 μL of GoTaq for 30 min at 72°C then cooled down to 25°C. Subassembly adaptor was generated by mixing 10 μL of 100 μM SC05, 10 μL of 100 μM SC06, and 40 μL H_2O, heating to 95°C, then ramping down to 25°C at 0.1 °C/s. T4 DNA ligase (20 min at 25°) was then used to ligate cleaned amplicons to a subassembly adaptor (3:1 adaptor:amplicon ratio), followed by heat inactivation for 10 min at 65°C. Standard Illumina cluster generators were appended to ligated products using 25 μL KAPA HiFI HotStart ReadyMix, 1 μL of the SC07 (10 μM) primer, 1 μL of the SC08 (10 μM) primer, 21 μL of H_2O, and 2 μL of 2 ng/mL ligated product using the following thermocycler conditions: 1 cycle for 3 min at 95°C, followed by 17 cycles of 98°C for 20 s, 62.4°C for 30 s, and 72°C for 1 min. A KAPA Library Quantification Kit (Kapa Biosystems) was used to quantify cluster-forming amplicons. A paired end MiSeq 300bp kit (Illumina)

Please cite this article in press as: Chakraborty et al., Profiling of drug resistance in Src kinase at scale uncovers a regulatory network coupling autoinhibition and catalytic domain dynamics, Cell Chemical Biology (2023), https://doi.org/10.1016/j.chembiol.2023.08.005

was used to sequence both the barcode and coding regions of each Src variant using both standard primers and the custom sequencing primer SC09. All reads sharing a common barcode sequence were collapsed to form a consensus, full-length Src variant sequence, resulting in 72,822 subassembled barcoded/Src variants. 31,728 of these 72,822 subassembled barcoded Src variants contained ''N''s, leaving 41,094 subassembled barcoded Src variants passing our initial filter.[20] A further quality filter (every nucleotide in Src required > = 5x reads) was then applied to these 41,094 subassembled barcoded Src variants, leaving a final of 25,390 high quality subassembled barcoded Src variants. These 25,390 barcodes represent 70% (~3500 mutants) of all possible single amino acid substitutions of Src's kinase domain, averaging 5 barcodes per single amino acid substitution of Src.

Src library transformation into yeast

Single colonies of freshly streaked BY4741 or BY4741 Green Monster were picked and grown in 5 mL of 2x transformation mix, YPAD (4% Peptone, 2% Bacto Dehydrated Yeast Extract, 0.008% Adenine sulfate, 2% glucose) overnight at 30°C. After overnight incubation, the culture was back diluted to an initial $O.D._{600}$ of 0.3 into 50 mL of 2x YPAD and then grown at 30°C until $O.D._{600}$ = 2. Then, the culture was centrifuged (3,000 xg) for 5 min. The subsequent pellet formed was washed with 25 mL of sterile H_2O (2x), resuspended in 1 mL of sterile H_2O, aliquoted equally into 10 eppendorf tubes, which were then pelleted at 17,000 xg for 30 s. Each pellet was then resuspended in transformation mix (240 mL of 50% PEG, 50 mL of 2 mg/mL Salmon Sperm (Invitrogen), 36 μL of 1M LiAc). 500 ng of BC Src library was added to eight of the pellets resuspended in transformation mix, 250 ng of BC Src library and 250 ng of pRS411 was added to one of the pellets resuspended in transformation mix, and H_2O vehicle was added to the remaining resuspended pellet. All transformations were incubated at 42°C for 45 min and then washed with 1 mL of sterile H_2O. The eight transformations containing 500 ng of BC Src library were pooled, added to 50 mL C-Leu 2% glucose, and then shaken at 30°C. Serial dilutions of this pooled culture were then plated on C-Leu plates to establish library size. Serial dilutions of the BC Src/pRS411 transformation were plated on C-Leu/Met plates to identify the percentage of double transformants. After 72 h of growth, aliquots of the pooled BC Src library were frozen in 20% glycerol at 80°C.

Inhibitor screening of Src variant library

Drug resistant screens for dasatinib were performed in the BY4741 strain, and for inhibitors **1**, **2**, and **4** in BY4741 Green Monsters. Aliquots of the frozen Src variant library were thawed and grown overnight at 30°C in C-Leu with 2% glucose. Cultures were then back diluted to an $O.D._{600}$ = 0.5 in C-Leu with 3% raffinose and allowed to double at least once. Selection was initiated by inoculation at $O.D._{600}$ = 0.01 in 250 mL C-Leu with 2% galactose. Samples prior to inhibitor selection were saved and served as timepoint = 0. Selection in presence of inhibitors was initiated by inoculation at a final $O.D._{600}$ of 0.01 into 200 mL C-Leu 2% galactose media ((dasatinib (25 or 100 μM), inhibitor **1** (8 μM), inhibitor **2** (2 μM), or inhibitor **4** (0.8 μM) were added during this step). Growth was monitored throughout the selection by measuring $O.D._{600}$. Selection $O.D._{600}$s are as follows; for 25 μM dasatinib: 0.22, 2.7, 11.7 (replicate #1) and 0.18, 2.1, 12.04 (replicate #2); 100 μM dasatinib: 0.26, 3.1, 11.6 (replicate #1) and 0.19, 2.2, 9.8 (replicate #2); for 8 μM of inhibitor **1**: 0.22, 0.65, 2.5 (replicate #1) and 0.39, 1.5, 5.2 (replicate #2); for 2 μM of inhibitor **2**: 0.18, 0.62, 4 (replicate #1) and 0.19, 0.83, 3.6 (replicate #2); for 0.8 μM of inhibitor **4**: 0.15, 1.2, 6.9 (replicate #1) and 0.32, 1.1, 3.6 (replicate #2). Yeast samples from all $O.D._{600}$ listed were harvested and pelleted at 3000 xg for 5 min and pellets were frozen at −80°C. Next, plasmids were extracted from frozen pellets using Yeast Plasmid Prep I (Zymogen) according to manufacturer's protocol and resuspended in 15 μL H_2O. To append Illumina cluster generators and append indices, 25 μL of 2x KAPA2G Robust HotStart ReadyMix (KAPA Biosystems), 2 μL of 10 mM SC10- SC12 (indexing primers), 2 μL of 10 mM SC13-SC17 (indexing primers), 13.5 μL of H_2O, and 7.5 μL of extracted plasmid. Thermocycler conditions used were: Initial denaturation at 95°C for 3 min, followed by 17 cycles of 95°C for 15 s, 60°C for 15 s, and 72°C for 15 s. Each amplification was cleaned (Zymo DNA Clean & Concentrator), quantified using KAPA Library Quantification Kit, then sequenced on NextSeq 500/550 High Output v2 kit (75 cycles) with standard Illumina sequencing primers and the custom primers SC18 and SC19.

Calculation of Src variant activity scores

Raw Illumina sequencing reads were processed and demultiplexed using bcl2fastq and ea-utils. The barcode map from subassembly step was used, with additional filtering of WT-associated barcodes (using 2x Std. Dev. of mean WT barcode activity score as a cutoff to filter out aberrantly acting WT barcodes). The activity scores of Src variants were then calculated using the Barcoded Variant SeqLib configuration with the ''Weighted Least Squares'' scoring option and ''Wild Type-like'' normalization in the Enrich2 software package.[21] For the four time points (t = 0 and 3 $O.D._{600}$ readings (listed in the inhibitor screening of Src variant library method)) in each inhibitor selection, the log ratio of each variant's frequency relative to the wild-type's frequency at the same time point was calculated. These log ratio values were regressed over time, and the inverse slope was used to assign an activity score for each Src variant. Inhibitors **1**, **2**, and **4** activity scores' were further quantile normalized to facilitate comparisons. Relates to Figures 1, S1, 2, S2, 3, S3, 4, S4, and S5.

Identifying resistance mutations

The Src variant library was treated with dasatinib or various conformation-selective inhibitors. Resistance mutations were identified based on variant activity score, where ''activity score'' equals the inverse of the Enrich2 output score. Upon inhibitor treatment, yeast harboring drug sensitive Src variants have their growth rescued, while those expressing drug resistant Src variants continue to grow poorly. Time points were sampled throughout growth, plasmids extracted, barcodes amplified and deeply sequenced on an

Please cite this article in press as: Chakraborty et al., Profiling of drug resistance in Src kinase at scale uncovers a regulatory network coupling autoinhibition and catalytic domain dynamics, Cell Chemical Biology (2023), https://doi.org/10.1016/j.chembiol.2023.08.005

Illumina NextSeq run as described above. We calculated the mean and standard deviation of activity scores for all synonymous variants identified in our dataset. A variant was classified as 'resistant' if its activity score was greater than 2x (dasatinib) or 3x (**1**, **2**, and **4**) the standard deviation from the mean activity score value of synonymous variants. Relates to Figures 1, S1, 2, S2, 3, and S3.

SH3 domain pulldown assays

SH3 pulldown experiment was performed as previously described.[14] Briefly, 20 μL of a 50% slurry of SNAP-capture pulldown resin (prepared using NHS-sepharose beads Fast-flow (4B)) was placed in a micro-centrifuge tube. The resin was washed (3x, 10 bead volumes) with pulldown buffer (20 mM Tris-HCl, pH 7.5, 100 mM NaCl, 1 mM DTT and 0.2 mg/mL BSA). 8 μM of SNAPtag–polyproline peptide fusion (VSLARRPLPPLP) was loaded onto the resin at a final volume of 50 μL per 10 μL of bead in pulldown buffer.[39] The resin was equilibrated at room temperature for 1 h and then washed (3x, 10 bead volumes) prior to performing pulldown assays.

Next, SH3 pulldown assays were performed with 100 nM of Src^{3D} (WT or W285T) or Src^{EEI} (WT or W285T) in 50 μL of pulldown buffer, incubated with 5 μL of the immobilized SH3 domain ligand. The resin-Src mixture was equilibrated at room temperature for 1 h on a rotator. Resin was spun down using a mini centrifuge, the supernatant was aspirated, and the resin was then washed three times before eluting the retained kinase with 50 μL of 1x SDS loading buffer. The beads were boiled at 95°C for 10 min. All samples were separated via SDS–PAGE and visualized by western blotting with Src antibody (Cell Signaling, #2109 for WT and #2102 for Src^{EEI}) on Li-Cor Odyssey. The scanned blots were quantified with ImageStudio Lite software and the signal corresponding to input protein ("I") was scaled to the original loaded kinase amount and signal corresponding to eluted ("E") was measured to determine kinase retained on the resin (% retained Src) based on the loaded and eluted fraction based on curve fitting of immunoblot signal intensity to a Src titration. Relates to Figures 4G and S4H.

Limited proteolysis of Src with thermolysin

Methods for limited proteolysis of Src was modified from previous work.[29] Briefly, Src^{3D} (WT, W285T, E283M, or E283D) or autoinhibited Src^{EEI} (WT, E283M, or W285T) was diluted to 1 μM in proteolysis buffer (50 mM Tris-HCl pH 8.0, 100 mM NaCl, 0.5 mM $CaCl_2$). Proteolysis was initiated by adding a 3.8 mM Thermolysin (Promega, #V4001) stock solution to the kinase (final concentration of thermolysin = 60 nM). 20 μL of this mixture was then added to 10 μL of 50 mM EDTA in 1x loading buffer to terminate proteolysis at various time points (0, 2, 4, 8, 16, 32, 64, 128, 256 min). The quenched samples were analyzed by SDS-PAGE (12% Bis-Tris gel in SDS running buffer) and stained with SYPRO Ruby (Thermo Fisher Scientific: #S12000) according to the manufacturer's protocol. Band intensities were analyzed by ImageStudioLite imaging software. The amount of Src remaining was normalized to the relative Src intensity band at 0 min and was plotted against time with GraphPad Prism 8.4.2. The curve was fit to an exponential decay equation using GraphPad Prism 8.4.2 software to obtain the half-life of each Src variant. Relates to Figures 4H, 4I, S4I, S4J, and S5B.

HDX-MS of Src

HDX-MS of Src was performed as described in previous work.[26] Briefly, purified Src^{3D} (WT or W285T) or Src^{CD} (WT or W285T) was diluted to 0.2 mg/mL in protein dilution buffer (50 mM HEPES, pH 7.8, 150 mM NaCl, 1 mM DTT, 5% glycerol). 10 μL of this dilution was then added to 90 μL of buffered D_2O (prepared 5 mL with 4.5 mL of D_2O and 0.5 mL of 10x protein dilution buffer and 0.2 μg/mL of peptide standard Glu-1-Fibrino peptide (CAS: 103213-49-6, Sigma)) to initiate deuteration at 22°C. Deuterium exchange was quenched after 3 s, 1 min, 30 min, and 20 h by adding the reaction to 100 μL of ice-cold quench buffer (0.2% formic acid, 8M Urea, 0.1% trifluoroacetic acid, allowing final pH to drop to 2.5) in order to lock deuterium in place and unfold the protein. All time points were collected in triplicate (except the 20 h samples of Src^{CD} which was collected in duplicate). Samples were immediately frozen in a dry ice/ethanol bath and stored at −80°C until LC-MS analysis. Undeuterated samples were prepared the same way except using buffered H_2O (Optima grade LC-MS water, Fisher Scientific, product #W6-4) instead of D_2O. Frozen samples were thawed on a 5°C block for 4 min prior to injection onto a loading loop. The loaded sample was passed over a custom-packed pepsin column (Porcine pepsin immobilized on POROS 20-AL resin; 2.1 × 50 mm column)[45] kept at 12°C with a flow of 0.1% trifluoroacetic acid (TFA) and 2% acetonitrile (ACN) at 200 μL/min. Digested peptic fragments were trapped onto a Waters XSelect CSH C18 XP VanGuard Cartridge (2.1 × 5 mm, 2.5 μm). After 5 min of loading, digestion, and trapping, peptides were resolved on an analytical column (Waters C18 BEH 1 × 100 mm, 1.7μm, 130 Å) using a gradient of 3%–40% solvent B for 9 min (A: 0.1% FA, 0.025% TFA, 2% ACN; B) 0.1% FA in ACN). The LC system was coupled to a Thermo Orbitrap performing full scans over the *m/z* range of 300–1500 at a resolution of 30,000. The MS source conditions were set to minimize loss.[46] Undeuterated samples were run prior to and at the end of all the LC-MS queues.

During the analytical separation step, a series of 250 μL injections were used to clean the pepsin column: 1) 0.1% Fos-12 with 0.1% TFA; 2) 2 M GndHCl in 0.1% TFA; 3) 10% acetic acid, 10% acetonitrile, 5% isopropanol.[47,48] After each gradient the trapping column was washed with a series of 250 μL injections: 1) 10% FA; 2) 30% trifluoroethanol; 3) 80% methanol; 4) 66% isopropanol, 34% ACN; 5) 80% ACN. During the trap washes the analytical column was cleaned with three rapid gradients.[49]

Peptic peptides were identified from data-dependent acquisition (DDA) experiments on undeuterated samples by exact mass and tandem mass spectrometry (MS/MS) spectra using Protein Prospector[50] filtering with a score cutoff of 15. Mass shifts were determined using HD-Examiner v2 (Sierra Analytics). The Glu-1-Fibrino internal standard peptide was checked in all samples to verify that back-exchange levels were consistent in all experiments.[51] Peptic peptides with significant differences in exchange were assessed using the hybrid significance threshold at 99% CI (Table S5) as well as consistency among all observed

overlapping peptides.[38] Based on this, the difference cut-off was set at 0.557 Da for Src^{3D} and 0.435 Da for Src^{CD}. All peptides that exceeded this cut-off were mapped in red onto the crystal structure of $Src.^{3D}$ Relates to Figure 5C and Table S5.

List of identified peptides as well as details of HDX exchange has been submitted as a Table S5.

Maleimide labeling and mass spectrometry

Purified 1 μM Src^{CD} (WT or W285T) was diluted in mass spectrometry buffer (50 mM HEPES, pH 7.6, 150 mM NaCl, 5% glycerol and 0.02% (w/v) n-Dodecyl β-D-maltoside (DDM))[52] and treated with 100 μM N-ethyl maleimide (NEM) in a LoBind 1.5 mL Eppendorf tube at 25°C for 30 min. The NEM labeling reaction was quenched with 20 mM of DTT in ammonium bicarbonate (NH_4HCO_3) solution. Protein was then precipitated using 0.02% deoxycholate and 10% trichloroacetic acid on ice for 10 min. The precipitated protein was pelleted by spinning at 10,000x rpm for 15 min. The pellet was dried with 10 μL acetone and resuspended in peptide solubilization buffer (8 M urea, 200 mM Tris-HCl, pH 8.0, 2.4 mM iodoacetamide (IA), 0.001% DDM) by vortexing briefly. The mixture was incubated in the dark for 30 min. Trypsin digestion solution (0.5 mg/mL of trypsin in 1 mM $CaCl_2$, 200 mM Tris-HCl, pH 8.0) was added and the protein was digested overnight at 37°C. Peptide was desalted using C-18 ZipTips (Milipore) and each sample was run on the Finnigan LTQ Ion trap. [M+3H]+3 peptide masses for both NEM and iodoacetamide modified, cysteine-containing peptide was analyzed using Xcalibur MaxQuant software. For each tryptic peptide (LGQGCFGEVW(T)MGTWNGTTR (P Loop) and AANILVGENLVCK (control)), the ion intensity for both the NEM-labeled and IA-labeled species were obtained, and a ratio was calculated. The experiment was repeated in triplicate. Relates to Figure 6E.

Synthesis of inhibitors

General Synthetic Procedures: All chemicals purchased from commercial suppliers were used without further purification unless otherwise stated. Reactions were monitored with thin-layer chromatography (TLC) using silica gel 60 F254 coated glass plates (EM Sciences). Compound purification was performed with an IntelliFlash 280 automated flash chromatography system using pre-packed Varian SuperFlash silica gel columns (hexanes/EtOAc or CH_2Cl_2/MeOH gradient solvent). A Varian Dynamax Microsorb 100-5 C18 column (250 mm × 21.4 mm), eluting with H_2O/CH_3CN or H_2O/MeOH gradient solvent (+0.05% TFA), was used for preparatory HPLC purification. The purity of all final compounds was determined by analytical HPLC with an Agilent ZORBAX SB-C18 (2.1 mm × 150 mm) or Varian Microsorb-MV 100-5 C18 column (4.6 mm × 150 mm), eluting with either H_2O/CH_3CN or H_2O/MeOH gradient solvent (+0.05% TFA). Elution was monitored by a UV detector at 220 nm and 254 nm, with all final compounds displaying >95% purity. Nuclear Magnetic Resonance (NMR) spectra were recorded on Bruker 300 or 500 MHz NMR spectrometers at ambient temperature.

Synthesis of 3-(4-amino-1-cyclopentyl-1*H*-pyrazolo[3,4-*d*ay]pyrimidin-3-yl)phenol (inhibitor 1)

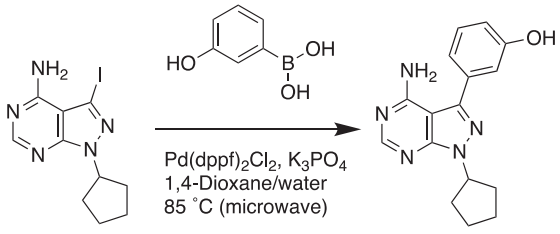

Inhibitor **1**

(3-Hydroxyphenyl)boronic acid (63 mg, 0.46 mmol, 1.5 equiv.) and 1-cyclopentyl-3-iodo-1H-pyrazolo[3,4-*d*ay]pyrimidin-4-amine (100 mg, 0.30 mmol, 1.0 equiv.) were dissolved in a mixture of 1,4-Dioxane (3.5 mL) and water (0.88 mL). Potassium phosphate (162 mg, 0.76 mmol, 2.5 equiv.) and bis(triphenylphosphine) palladium(II) dichloride (25 mg, 0.030 mmol, 10%) were added. The resulting mixture was then heated at 85°C for 2 h in a microwave reactor. After cooling, the reaction was diluted with EtOAc (40 mL) and quenched with saturated aqueous NH_4Cl solution (10 mL). The organic phase was separated and washed with brine, dried over anhydrous Na_2SO_4. Flash chromatography on silica gel (eluted with a gradient of 0%–100% of EtOAc in hexanes) afforded 3-(4-amino-1-cyclopentyl-1*H*-pyrazolo[3,4-*d*ay]pyrimidin-3-yl)phenol as a pale yellow solid (67 mg, 76%). ^{1}H-NMR (500 MHz, $CDCl_3$) δ 8.29 (s, 1H), 7.36–7.29 (m, 1H), 7.00–6.94 (m, 2H), 6.83–6.77 (m, 1H), 5.31 (p, J = 8.0 Hz, 1H), 2.23–2.14 (m, 4H), 2.03–1.95 (m, 2H), 1.80–1.69 (m, 2H); MS (ESI, m/z) calculated for $C_{16}H_{17}N_5O$ 295.1, $[M + H]^+$ found 296.4; HPLC purity: >97%. Relates to Figures 3 and 4, S1, and S3.

Please cite this article in press as: Chakraborty et al., Profiling of drug resistance in Src kinase at scale uncovers a regulatory network coupling auto-inhibition and catalytic domain dynamics, Cell Chemical Biology (2023), https://doi.org/10.1016/j.chembiol.2023.08.005

Synthesis of 1-cyclopentyl-3-(4-phenoxyphenyl)-1*H*-pyrazolo[3,4-*d*ay]pyrimidin-4-amine (inhibitor 2)

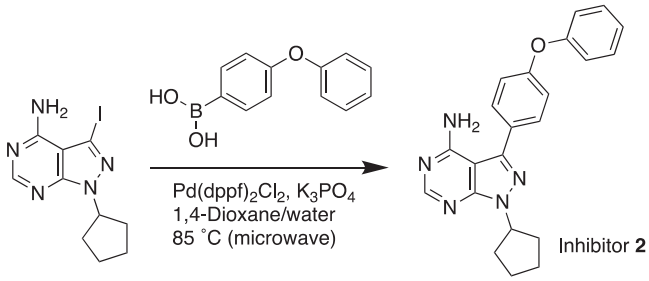

4-Phenoxyphenylboronic acid (98 mg, 0.46 mmol, 1.5 equiv.) and 1-cyclopentyl-3-iodo-1H-pyrazolo[3,4-*d*ay]pyrimidin-4-amine (100 mg, 0.30 mmol, 1.0 equiv.) were dissolved in a mixture of 1,4-Dioxane (3.5 mL) and water (0.88 mL). Potassium phosphate (162 mg, 0.76 mmol, 2.5 equiv.) and bis(triphenylphosphine) palladium(II) dichloride (25 mg, 0.030 mmol, 10%) were added. The resulting mixture was then heated at 85°C for 2 h in a microwave reactor. After cooling, the reaction was diluted with EtOAc (40 mL) and quenched with saturated aqueous NH_4Cl solution (10 mL). The organic phase was separated and washed with brine, dried over anhydrous Na_2SO_4. Flash chromatography on silica gel (eluted with a gradient of 0%–90% of EtOAc in hexanes) afforded 1-cyclopentyl-3-(4-phenoxyphenyl)-1H-pyrazolo[3,4-*d*ay]pyrimidin-4-amine as a pale yellow solid (93 mg, 82%). ^{1}H-NMR (500 MHz, $CDCl_3$) δ 8.25 (s, 1H), 7.59 (d, J = 8.6 Hz, 2H), 7.44–7.39 (m, 1H), 7.28–7.20 (m, 2H), 7.17 (d, J = 8.5 Hz, 2H), 7.10 (d, J = 7.7 Hz, 2H), 5.36–5.27 (m, 1H), 2.26–2.12 (m, 4H), 2.10–1.93 (m, 4H); MS (ESI, m/z) calculated for $C_{22}H_{21}N_5O$ 371.2, $[M + H]^+$ found 372.2; HPLC purity: >99%. Relates to Figures 3 and 4, S1, and S3.

Synthesis of *N*-(3-ethynyl-4-methylphenyl)-3-(trifluoromethyl)benzamide

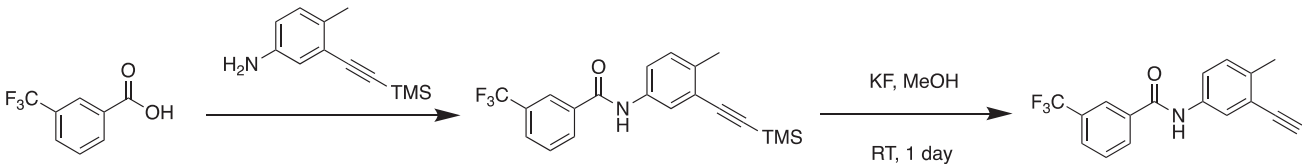

4-Methyl-3-((trimethylsilyl)ethynyl)aniline (1.0 g, 4.9 mmol, 1.0 eq.), 3-trifluomethyl-benzoic acid (1.4 g, 7.4 mmol, 1.5 eq.) and HOAt (1.0 g, 7.4 mmol, 1.5 eq.) were dissolved in dry DMF (20 mL). The solution was cooled on ice and to it was added 1-Ethyl-3-(3-dimethylaminopropyl) carbodiimide (1.4 g, 7.4 mmol, 1.5 eq.). The reaction mixture was then allowed to warm to room temperature overnight. The solvent was removed in vacuo and the solid residue was dissolved in EtOAc (200 mL). The organic layer was washed with a saturated aqueous KH_2PO_4 solution (30 mL), a saturated aqueous $NaHCO_3$ solution (30 mL), brine (30 mL), and dried over anhydrous Na_2SO_4. The solvent was removed in vacuo and the solid residue was dissolved in dry MeOH (30 mL). Potassium fluoride (1.3 mg, 22 mmol, 4.5 eq.) was added and the resulting mixture was stirred at room temperature for 1 day. The reaction mixture was then filtered and concentrated in vacuo. The solid residue was dissolved in EtOAc (200 mL) and washed with water (20 mL), brine (30 mL) and dried over anhydrous Na_2SO_4. Purification by flash chromatography with silica gel afforded N-(3-ethynyl-4-methylphenyl)-3-(trifluoromethyl)- benzamide as a pale brown solid (0.98 g, 66% for two steps). ^{1}H-NMR (500 MHz, $CDCl_3$) δ 8.10 (s, 1H), 8.03 (d, J = 7.7 Hz, 1H), 7.90 (s, 1H), 7.80 (d, J = 7.8 Hz, 1H), 7.69 (s, 1H), 7.61 (t, J = 7.8 Hz, 1H), 7.56 (d, J = 8.2 Hz, 1H), 7.20 (d, J = 8.3 Hz, 1H), 3.28 (s, 1H), 2.43 (s, 3H); ^{13}C-NMR (126 MHz, $CDCl_3$) δ 164.44, 137.73, 135.68, 135.10, 131.44, 130.50, 130.28, 129.61, 128.61, 124.40, 124.13, 123.75, 122.73, 121.30, 81.98, 81.62, 20.22; MS (ESI, m/z) calculated for $C_{17}H_{12}F_3NO$ 303.1, $[M + H]^+$ found 304.1.

Please cite this article in press as: Chakraborty et al., Profiling of drug resistance in Src kinase at scale uncovers a regulatory network coupling autoinhibition and catalytic domain dynamics, Cell Chemical Biology (2023), https://doi.org/10.1016/j.chembiol.2023.08.005

Synthesis of *N*-(3-((4-amino-1-cyclopentyl-1*H*-pyrazolo[3,4-*d*ay]pyrimidin-3-yl)ethynyl)-4-methylphenyl)-3-(trifluoromethyl)benzamide (inhibitor 3)

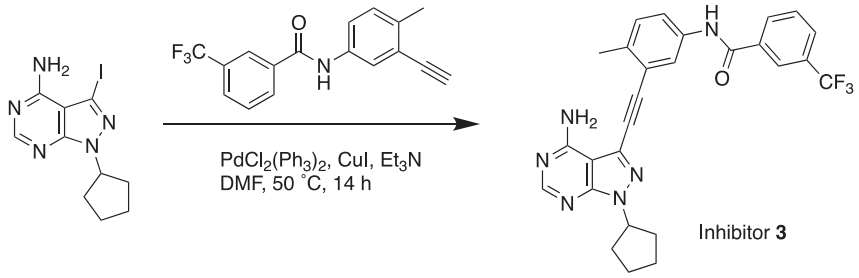

1-Cyclopentyl-3-iodo-1H-pyrazolo[3,4-*d*ay]pyrimidin-4-amine (100 mg, 0.30 mmol, 1.0 eq.) was dissolved in anhydrous DMF (4 mL) and the solution was flushed with a moderate stream of nitrogen for 5 min. Triethylamine (124 mg, 1.2 mmol, 4.0 eq., 167 μL), *N*-(3-ethynyl-4-methylphenyl)-3-(trifluoromethyl)-benzamide (138 mg, 0.46 mmol, 1.5 eq.), bis(triphenylphosphine)palladium(II) dichloride (11 mg, 0.015 mmol, 5.0%) and copper(I) iodide (5.8 mg, 0.030 mmol, 10%) were added sequentially. The resulting mixture was heated at 50°C for 14 h and then diluted with EtOAc (40 mL). The organic phase was washed with a saturated aqueous NH_4Cl solution (10 mL), brine, dried over anhydrous Na_2SO_4 and concentrated in vacuo. Purification with flash chromatography using a gradient of 0%–90% of EtOAc in hexanes afforded N-(3-((4-amino-1-cyclopentyl-1H-pyrazolo[3,4-*d*ay]pyrimidin-3-yl)ethynyl)-4-methylphenyl)-3-(trifluoromethyl) benzamide as a pale yellow solid (120 mg, 78%). ^{1}H-NMR (500 MHz, $CDCl_3$) δ 8.72 (s, 1H), 8.26 (s, 1H), 8.23 (d, J = 7.7 Hz, 1H), 8.05 (s, 1H), 7.88 (d, J = 8.0 Hz, 1H), 7.74 (d, J = 7.4 Hz, 1H), 7.60 (t, J = 7.6 Hz, 1H), 7.24 (d, J = 8.4 Hz, 1H), 5.34–5.23 (m, 1H), 2.49 (s, 3H), 2.28–2.09 (m, 4H), 2.09–1.97 (m, 2H), 1.85–1.72 (m, 2H); MS (ESI, m/z) calculated for $C_{27}H_{23}F_3N_6O$ 504.2, $[M + H]^+$ found 505.6; HPLC purity: >99%. Relates to Figures 3 and 4.

Synthesis of *N*-(3-((4-amino-1-methyl-1*H*-pyrazolo[3,4-*d*ay]pyrimidin-3-yl)ethynyl)-4-methylphenyl)-3-(trifluoromethyl)benzamide (inhibitor 4)

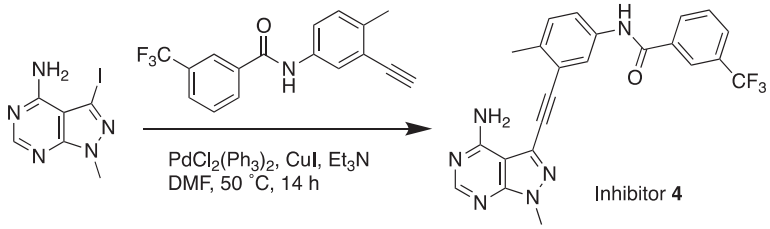

3-Iodo-1-methyl-1H-pyrazolo[3,4-*d*ay]pyrimidin-4-amine (73 mg, 0.27 mmol, 1.0 eq.) was dissolved in anhydrous DMF (3.5 mL) under nitrogen. Triethylamine (110 mg, 150 μL, 1.1 mmol, 4.0 eq.), *N*-(3-ethynyl-4-methylphenyl)-3-(trifluoromethyl)-benzamide (120 mg, 0.40 mmol, 1.5 eq.), bis(triphenylphosphine) palladium(II) dichloride (9.3 mg, 0.013 mmol, 0.05 eq.), and copper (I) iodide (5.1 mg, 0.027 mmol, 0.10 equiv.) were added to the above solution sequentially. The reaction was heated at 50°C for overnight under nitrogen and then quenched with a saturated NH_4Cl aqueous solution (5 mL). The resulting mixture was diluted with ethyl acetate (40 mL) and the organic phase was washed with a saturated $NaHCO_3$ aqueous solution (10 mL), brine (10 mL), and then dried over anhydrous Na_2SO_4. Purification by flash chromatography on silica gel using a gradient of 0%–100% of EtOAc in hexanes afforded inhibitor **4**,*N*-(3-((4-amino-1-methyl-1H-pyrazolo[3,4-*d*ay]pyrimidin-3-yl)ethynyl)-4-methylphenyl)-3-(trifluoromethyl)benzamide as a pale brown solid (70 mg, 58%). ^{1}H-NMR (300 MHz, DMSO) δ = 10.57 (s, 1H), 8.43–8.27 (m, 3H), 8.09 (s, 1H), 8.01 (d, J = 7.6 Hz, 1H), 7.92–7.74 (m, 2H), 7.39 (d, J = 8.5 Hz, 1H), 3.98 (s, 3H), 3.39 (s, 3H), 2.53 (s, 2H); MS (ESI, m/z) calculated for $C_{23}H_{17}F_3N_6O$ 450.1, $[M + H]^+$ found 451.1. HPLC purity >99%. Relates to Figures 3, S1, and S3.

QUANTIFICATION AND STATISTICAL ANALYSIS

For all statistical tests (unless otherwise noted), a two-tailed Student's *t* test was used to compare means between two samples. A one-way ANOVA with post hoc Tukey's HSD test was used to compare means between more than two samples. Statistical tests were performed in R or GraphPad Prism 8.4.2. SEM for n = 3–6 has been reported for all *in vitro* biochemical assays. Significance is denoted as * = $p < 0.05$, *** = $p < 0.001$, **** = $p < 0.0001$.

Please cite this article in press as: Chakraborty et al., Profiling of drug resistance in Src kinase at scale uncovers a regulatory network coupling auto-inhibition and catalytic domain dynamics, Cell Chemical Biology (2023), https://doi.org/10.1016/j.chembiol.2023.08.005

Calculation of K_I, IC_{50} and K_M

IC_{50} values were calculated in GraphPad Prism using the ''One-Site Fit log IC50.'' K_M [ATP] values were determined using GraphPad Prism using ''Plot Michaelis-Menten'' option. K_I values for all Src constructs were calculated using the Cheng-Prusoff equation at 1 mM ATP and calculated K_M [ATP]. Relates to Figures 3D, S3G, 4B, and S4G.

Calculation of Src phosphotransferase activity

Slopes were calculated from the linear portion of *in vitro* kinase enzyme assay to first obtain raw fluorescence count per sec. This was then divided by fluorescence change per picomoles of phosphorylated substrate (obtained from the slope of a standard curve of raw fluorescence versus phosphorylated substrate) to calculate phosphorylated substrate produced in pmoles sec^{-1} reported per nM of the Src variants tested. Relates to Figures S3G, 4D–4F and 6D.